

AUS Repository

Modeling, design, and implementation of a bio-inspired propulsion mechanism for underwater vehicles

Item Type	Thesis
Authors	Omari, Mohamad
Download date	2026-04-16 10:39:39
Link to Item	http://hdl.handle.net/11073/21519

MODELING, DESIGN, AND IMPLEMENTATION OF A
BIO-INSPIRED PROPULSION MECHANISM FOR
UNDERWATER VEHICLES

by

Mohamad Omari

A Thesis presented to the Faculty of the
American University of Sharjah
College of Engineering
In Partial Fulfillment
of the Requirements
for the Degree of

Master of Science in
Mechatronics Engineering

Sharjah, United Arab Emirates

April 2021

Declaration of Authorship

I declare that this thesis is my own work and, to the best of my knowledge and belief, it does not contain material published or written by a third party, except where permission has been obtained and/or appropriately cited through full and accurate referencing.

Signed.....Mohamad Omari.....

Date.....13/4/2021.....

The Author controls copyright for this report.

Material should not be reused without the consent of the author. Due acknowledgement should be made where appropriate.

© Year 2021

Mohamad Omari

ALL RIGHTS RESERVE

Approval Signatures

We, the undersigned, approve the Master's Thesis of Mohamad Omari

Thesis Title: Modeling, design, and implementation of a bio-inspired propulsion mechanism for underwater vehicles

Date of Defense: April 29, 2021

Name, Title and Affiliation

Signature

Dr. Mehdi Ghommem
Associate Professor, Department of Mechanical Engineering
Thesis Advisor

Dr. Lotfi Romdhane
Professor, Department of Mechanical Engineering
Thesis Co-Advisor

Dr. Mohammad Omar Hamdan
Professor, Department of Mechanical Engineering
Thesis Committee Member

Dr. Mohammad Jaradat
Professor, Department of Mechanical Engineering
Thesis Committee Member

Dr. Mohammad Jaradat
Coordinator
Mechatronics Engineering Program

Dr. Lotfi Romdhane
Associate Dean of Graduate Affairs and Research
College of Engineering

Dr. Sameer Al-Asheh
Interim Dean
College of Engineering

Dr. Mohamed El-Tarhuni
Vice Provost for Graduate Studies
Office of Graduate Studies

Acknowledgement

First and foremost, I thank Allah and I ask his aid in this work of mine. I would like to express my deepest appreciation to my thesis advisor; Dr. Mehdi Ghommem, for his role as both a thesis advisor and a mentor during my studies. Dr. Mehdi's persistent feedback and support are the cornerstone upon which this thesis is built. I would like to also thank my Co-advisor, Dr. Lotfi Romdhane, for firstly guiding me to this opportunity and for his continued feedback and support, on both a scientific and moral level. I would like also to thank my thesis committee members; Dr. Mohammad Jaradat and Dr. Mohammed Hamdan for their valuable comments and advice, both in the proposal and in the defense. At last, my sincere thanks to the American University of Sharjah and the Mechatronics Engineering Program for granting me a Graduate Research Assistantship (GRA) to pursue my studies. A final thanks to all the workers, academics, administrators, and employees in the American University of Sharjah whose individual contributions are akin to gears in a large, complex, mechanism.

Dedication

In the name of Allah, the most gracious, the most merciful

*I thank my family, whose support to me is akin to an anchoring pillar in a
raging sea*

I thank my friends, for their continuing kindness and helpful advice

Abstract

Recent advances in bio-robotics research and smart materials have boosted the development of bio-inspired autonomous underwater vehicles (AUVs) to replace their conventional counterparts driven by rotary propellers. These vehicles can serve in several applications including marine environment exploration, search and rescue, military surveillance, and border patrol. In this Thesis, we investigate the hydrodynamic performance of robotic fish tail inspired from three different fish species, namely the big-eye trevally, the butterfish, and the boxfish. A detailed CAD model of the robotic fish is developed and simulated using the MATLAB tool Simscape Multibody. The bio-inspired propulsion mechanism consists of three articulated segments actuated by servomotors and a caudal fin to produce the desired fish wavy motion. A testing platform, equipped with load cell and distance laser sensor, is developed to measure the produced thrust and associated forward speed over a range of undulation frequencies and lateral amplitude of tail oscillations. The experimental results showed good agreement with Lighthill's theory of elongated-body propulsion. Then, a comparative study is conducted to examine the swimming capabilities of the aforementioned fish species. The boxfish was found the slowest of the three species, with a mean thrust of 6.46 mN and a forward speed of 10.2 cm/s. This reflects the characteristics of the boxfish being a reef fish, which is best suited for tight maneuvering and bursts of speed rather than a long sustained cruising speed. The trevally is observed to produce the fastest swimming with an estimated forward speed of 25.2 cm/s. The experimental results are also compared to previous studies on robotic fish reported in the literature.

Keywords: Robotic fish, undulatory deformation, bio-inspired propulsion, swimming performance.

Table of Contents

Abstract.....	6
List of Figures.....	9
List of Tables.....	11
List of Abbreviations.....	12
Chapter 1. Introduction.....	13
1.1 Background of Research.....	13
1.2 Thesis Objectives.....	13
1.3. Research Contribution.....	14
1.4. Thesis Organization.....	14
Chapter 2. Background and Literature Review.....	15
2.1 Motion Profile Generation.....	15
2.1.1 Body caudal fin propulsion.....	16
2.1.2 Median paired fin propulsion.....	17
2.1.3 Body wave control.....	18
2.1.4 Central pattern generation method of control:.....	20
2.2 Actuation Solutions.....	22
2.2.1. Motor based fish designs.....	22
2.2.2 Smart materials based actuation.....	24
2.3 Designs for Experimental Apparatus.....	26
Chapter 3. Methodology.....	28
3.1. Ideal Body Wave Selection and Discretization.....	28
3.1.1 Morphological selection.....	28
3.1.1.1 Carangidae selection.....	29
3.1.1.2 Pholidae selection.....	30
3.1.1.3 Ostraciidae selection.....	31
3.1.2 Ideal body wave discretization.....	32
3.2. The Robotic Fish Dynamic Model.....	36
3.2.1 Rigid body kinematics.....	36
3.2.2 Thrust and forward speed models.....	43

3.2.3 Robotic fish dynamic model	43
Chapter 4. Experimental Setup	46
4.1 The Robotic Fish Design	46
4.2 The Experimental Set-up Design	48
Chapter 5. Results and Analysis	51
5.1 Experimental Verification.....	51
5.2 Comparative Swimming Performance Analysis	53
Chapter 6. Conclusion and Future Work	58
References.....	60
Vita	66

List of Figures

Figure 2.1 Types of swimming motion based on undulation or oscillation of a) tails or b) fins [5].....	16
Figure 2.2 Carmen and anti-Carmen vortices in BCF motion [6]	16
Figure 2.3 A multilink fish-based design vs an Ideal Body Wave	19
Figure 2.4 ANSYS simulations of the NACA airfoil being used for the aerodynamic profile [14]	20
Figure 2.5 The Robotuna design schematic [34]	23
Figure 2.6 Zhang’s Carangiform robotic fish CAD model [6]	24
Figure 2.7 The actuation of an IPMC [37].....	25
Figure 2.8 IPMC propelled robotic fish [38]	25
Figure 2.9 Untethered robotic fish actuated by MFC a) modeled view; (b) side view; (c) top view; and (d) combined motion capture with turning motion. Swimming speed when under actuation voltage of amplitude 1000 V at 5 Hz is approximately 7.5 cm/s [39]	26
Figure 2.10 An example of a static tail testing apparatus [37]	27
Figure 3.1 A picture of the Bigeye Trevally in the wild [41]	29
Figure 3.2 The ideal body wave of a bigeye trevally extracted.....	30
Figure 3.3 The discretization of the ideal body wave and a visual display of S_{sum} ..	33
Figure 3.4 The discretization of the ideal body wave.....	34
Figure 3.5 The numerical method of finding the fish motion visualized, where θ represents the angle relative to the previous link, and γ represents the absolute angle with respect to the global x-axis.....	35
Figure 3.6 Coordinate frames of the discretized ideal body wave.....	37
Figure 3.7 A diagram of the control architecture within the servo motors [52]	40
Figure 3.8 The input angles vs the output.....	41
Figure 3.9 Undulatory motion of robotic fish: Simscape simulations.	42
Figure 3.10 Tip trajectories: comparison between analytical model and Simscape Multibody. The X and Y coordinate system directly correspond to x and $h(x, t)$ as defined in Section 2	43
Figure 3.11 Representation of the hydrodynamic forces applied on the robotic fish (planar motion). Schematic adopted from [40], [54].	45

Figure 4.1 CAD model of the robotic fish.....	47
Figure 4.2 The experimental set up.....	49
Figure 5.1 Time variations of the caudal fin position: measurements vs. analytical model. Results are shown for two different undulation frequencies.....	51
Figure 5.2 Variations of the mean thrust with the undulation (a) frequency and (b) angle amplitude: experiments vs. Lighthill's theory.	53
Figure 5.3 Variations of the mean forward speed with the undulation (a) frequency and (b) angle amplitude.	53
Figure 5.4 Locomotion of three fishes under investigation from left to right boxfish, butterflyfish, and trevally.	54
Figure 5.5 Time variations of the thrust of the three fish models: (a) boxfish, (b) butterflyfish, and (c) trevally. Dashed line indicates the mean value of the thrust.	55
Figure 5.6 Forward speed vs. length of robotic fish length: comparison against previous studies reported in the literature [61]–[80].	57

List of Tables

Table 3.1 The optimized Link Lengths.....	33
Table 3.2 The DH parameters of the robotic fish	39
Table 3.3 The PID gains for the dynamixel servo motors	40
Table 3.4 Numerical values of hydrodynamic constants used in the estimate of the forward speed of the robotic fish obtained as a half streamline body from [45].	45
Table 4.1 A general design table for the robotic fish.....	48
Table 5.1 Swimming performance of the three fish models.....	56

List of Abbreviations

AUV	Autonomous Underwater Vehicle
BCF	Body-Caudal Fin
CPG	Central Pattern Generation
IPMC	Ionic Polymer-Metal Composite
MFC	Macro Fiber Composite
MPF	Median Paired Fin
NACA	National Advisory Committee for Aeronautics
PID	Proportional Integral Derivative
PWM	Pulse Width Modulation

Chapter 1. Introduction

1.1 Background of Research

Naval architecture and marine exploration are one of the most complex fields of engineering, with applications in search and rescue, marine life documentation, and border patrol. Naval vessels actuation methods have experienced many evolutions throughout history, evolving from sails to the modern-day screw propeller method of actuation, which drives the majority of modern naval vessels today. The current methods of naval actuation, however, are far inferior to those deployed by fish, whose swimming efficiency is observed to be around 90% for most species [1]. This is mostly due to the fish body morphology. Formed over millennia of evolution, the fish morphology allows them to perform complex tasks and maneuvers in adverse aquatic environments. Therefore, researchers have adopted designs that emulate fish's biological functions in multiple ways that can be grouped under two subcategories: Biomimicry and Bio-inspiration. Biomimicry takes a bottom-up approach to design, adopting aspects of the fish akin to biological cells and aims to impart biological functionalities within the modeled design. Bio-inspiration is the polar opposite, taking a bottom-up approach to design and adopting certain functionalities and morphologies within a selected species while utilizing non-organic hardware such as motors, microcontrollers, and location sensors [2]. In the present research, we selected a bio-inspiration route due to the overwhelming complexity associated with the development of biological cells. It should also be noted that not all morphological functions within fish are a global optimum, as fish usually tend to optimize their function based on their environment and mission [3].

1.2 Thesis Objectives

The Thesis is primarily concerned with building, testing, modeling, and performance analysis of bio-inspired propulsion mechanisms based on three fish species, namely the big-eye trevally, the butterfish, and the boxfish. These species possess different morphologies, motion forms, and performance requirements. The propulsion mechanism is based on three rigid segments linked in series and driven by servomotors to deform the posterior end of the robot based on desired fish body

deformation. This end includes a bioinspired passive caudal fin. The main objectives of the Thesis are:

- Model and simulate bio-inspired propulsion mechanisms based on different fish species.
- Implement undulatory/oscillatory fish motion using articulated segments actuated by servomotors.
- Develop a testing set-up for motion and hydrodynamic force measurements.
- Analyze the swimming capabilities of fish robots inspired from different fish species.

1.3. Research Contribution

The contributions of this research work can be summarized as follows:

- The development of a methodology that can extract the motion of fish species, analyze it and translate it into a set of inputs and parameters for an appropriate rigid link robotic fish design.
- The development of a hydrodynamic model, which incorporates added mass effect and Lighthill theory of elongated bodies.
- The design and development of an experimental testing apparatus to assess the robotic fish tail's swimming performance.
- A comparative analysis of the swimming performance of multiple fish species using the developed robotic fish tail.

1.4. Thesis Organization

This Thesis is organized as follows. Chapter 2 reviews different types of robotic fish, their motion profiles, different methods of control, and different models and designs. Chapter 3 covers the design methodology including the selection of the motion profiles based on morphology and their discretization, the hydrodynamic model and its implementation. The results and comparison with theory and previously reported data are presented in Chapter 4. Chapter 5 contains concluding remarks and suggestions for future research work.

Chapter 2. Background and Literature Review

Robotic fish design is a relatively recent field of robotics, as the exploration of aquatic animal motion was only pursued at the onset of the 20th century. The cornerstone of robotic fish design was founded by Charles Marcus Breder in 1926, where his work categorized the swimming motion of fish to be of two types based on their temporal features [4]:

- 1) Periodic swimming: assumes that some fish move in a cyclic manner, where propulsion occurs at constant speed to cover large distances at high efficiency.
- 2) Unsteady swimming: denotes the escape, maneuvers, and turning motions of fish. This type of movement is used for foraging, escaping predators, and hunting prey.

These classifications are noted to be a simple representation in the modern day, as the push for better emulation of fish motion has resulted in a plethora of literature concerning fish modeling and simulation. All the corpus of literature concerning robotic design can be classified into five areas: 1) motion profile generation 2) mathematical modeling and simulation of the locomotion and body kinematics 3) close biomimicry of fish morphology and design 4) methods of actuation and current models of robotic fish 5) examination of existing experimental apparatus for robotic fish testing.

2.1 Motion Profile Generation

The motion profile of a fish's movement maybe the most prolific of aspects that concern robotic fish design, as it dictates the level of noise, speed, maneuvering motions, and bio-mimicry. The most important aspects of fish tail motion and the level of dexterity, speed, and maneuverability it exhibits were classified by Sfakiotakis et al [5]. In their work, they mentioned that the fish tail's motion can range from undulatory to oscillatory, which denotes the number of waves on the fish motion from N number of waves to less than half. The classification also denotes the length of the tail with respect to the body. This parameter constitutes an important aspect in robotic fish design which allows the designer to designate priority to the most important parts of fish swimming in terms of maneuverability and speed [5].

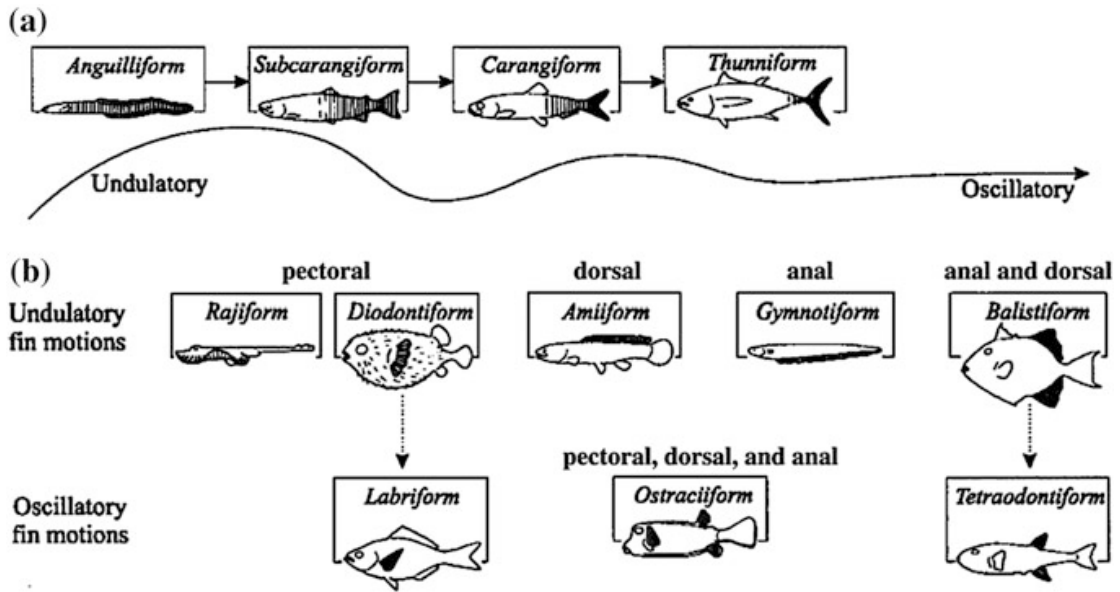


Figure 2.1 Types of swimming motion based on undulation or oscillation of a) tails or b) fins [5]

2.1.1 Body caudal fin propulsion As indicated by Figure 2.1, a fish's method of propulsion can be classified under one of two subcategories: A Body Caudal Fin propulsion (BCF), and Median and/or Paired Fin Mode (MPF). The BCF motion is where the fish relies on its body wave and a passive caudal fin to actuate its movement in water. The motion is generated by a propulsive wave through the tail that moves opposite to the direction of motion, generating a Carmen vortex in the direction of the water flow. The drainage effect resulting from the Carmen vortex generates an opposing vortex called the anti-Carmen vortex, which moves parallel to the tail and provides a high propulsive efficiency [6].

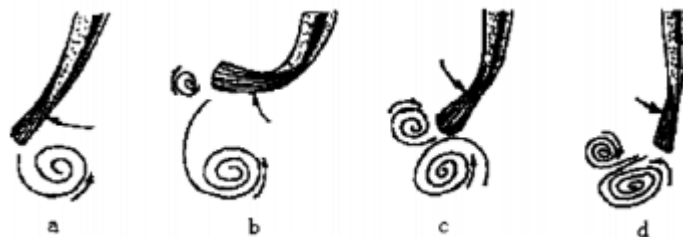


Figure 2.2 Carmen and anti-Carmen vortices in BCF motion [6]

Thus, it can be determined that the motion generation in BCF robotic fish relies nearly entirely on the waveform of the tail and its respective length. Indeed, an important factor in this type of fish motion is determined by the ratio of the tail length over the body length [7]. BCF swimming mode is observed to enable fish a high level

of forward speed and acceleration at high efficiency at the cost of maneuverability and turning motion, and with more than 85% of known fish species exhibiting this method of motion [8], [9]. As such, BCF motion has been widely adopted by the research community, as its relative simplicity in comparison with MPF as well as the demonstrable swimming speed governed by measurable parameters that can be optimized in several ways (more on details on this will be presented in section 2.1).

2.1.2 Median paired fin propulsion An MPF motion mainly relies on the fins of the fish for motion while minimally integrating the tail's propulsive motion. While BCF motion relies on the tail length of the fish with respect to the body and the waveform of the tail, MPF motion is based on the fins oscillations and its respective waveform. The fin that acts as the primary method of propulsion determines the type of swimming motion that the fish exhibits and the generated hydrodynamic loads [10]. The most common MPF motion is the labriform, which relies on pectoral fins and has a significant body of work covering it in comparison to other MPF motions. Labriform motion has two main oscillatory type motions: a rowing motion (relying on drag) [11], and a flapping motion (relying on lift) [12].

Due to the complexity associated with body kinematics and the hydrodynamic interactions with fins, MPF motion has only recently received attention from the research community. These complexities come in addition to the fact that MPF prioritizes maneuverability over speed, which is a harder parameter to quantify than the fish forward velocity. While the different swimming configurations do not hinder species in areas they are not specialized in (i.e. tuna fish which travels at high speeds still retains a high degree of maneuverability), they have a much more marked effect on robotic fish and their level of movement [7]. Indeed, Breder [4] stated regarding fish swimming modes that "Fish may exhibit more than one swimming mode, either at the same time or at different speeds. Median and paired fins are routinely used in conjunction to provide thrust with varying contributions from each, achieving smooth trajectories".

The three most prolific methods of motion profile generation in robotic fish are the body wave based control mode [8] and the central pattern generation control mode [9]. Body-wave control relies on taking the overall shape of the fish's body motion and approximating it using a mathematical model which result in motion inputs to the robot

(such as servo angles or voltage frequencies). Central Pattern Generation aims to emulate a fish action by utilizing a biological neural network to control a fish posture in accordance to the environment rather than based on ideal wave shape [13].

2.1.3 Body wave control Body-wave control can be estimated in multiple methods, the most common of which is the BCF function. The BCF function, as shown in Equation (1), uses the tip movement of the tail to estimate the body wave shape [6].

$$y_{body} = (C_1x + C_2x^2) \sin(kx + \omega t) \quad (1)$$

where y_{body} is the envelope of the fish body and C_1 is the primary coefficient and C_2 is the quadratic coefficient k is the body wave number ($k = \frac{2\pi}{\lambda}$), and ω is the wave's frequency ($\omega = 2\pi f = \frac{2\pi}{T}$). The wave number and frequency can be determined from the designer's desired torque and speed of actuation, which are calculated using mathematical models like the Lighthill formula or the Taylor's resistive method. The formula can also be discretized to suit a multi-rigid link [1], which allows the roboticist to automate their motion using an oscillatory tail part made of an N number links, connected in series, with endpoints that match the ideal body wave.

$$y_{body}(x, i) = (C_1x + C_2x^2) \sin(kx \pm 2\omega_{body}t) \quad (2)$$

where the variable i denotes the i^{th} sequence of y_{body} in the oscillation period, and ω_{body} is the wave frequency, and k is denoted as the body wave number. Increasing body wave number k changes the swimming from oscillatory to undulatory. The (\pm) sign is dependent upon the initial direction of the movement of the tail.

A more complex alternative to the discretized version of body formula is to numerically fit the points with the length of the respective chains to the ideal body wave. While the discretized version of the body wave is not free of errors, the oscillation constitutes a good approximation to the ideal body wave as shown in Figure 2.3. The ideal body wave displayed here is that of a Carangiform robotic fish discretization which will be explained in a later section. Namely said section is 3.1.2, titled "Ideal Body Wave Discretization". The section goes into this thesis's method to obtain the motor input to the robotic fish from the ideal body wave of multiple potential species which uses a BCF motion.

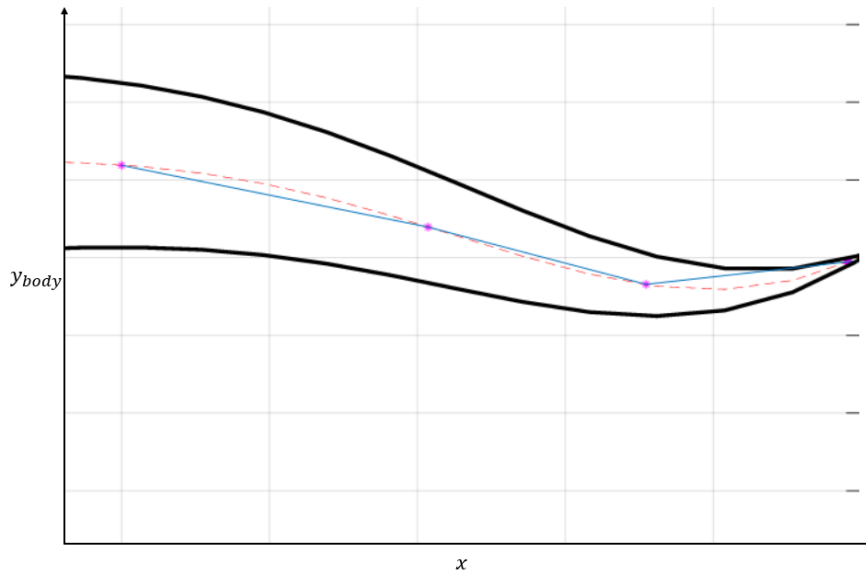
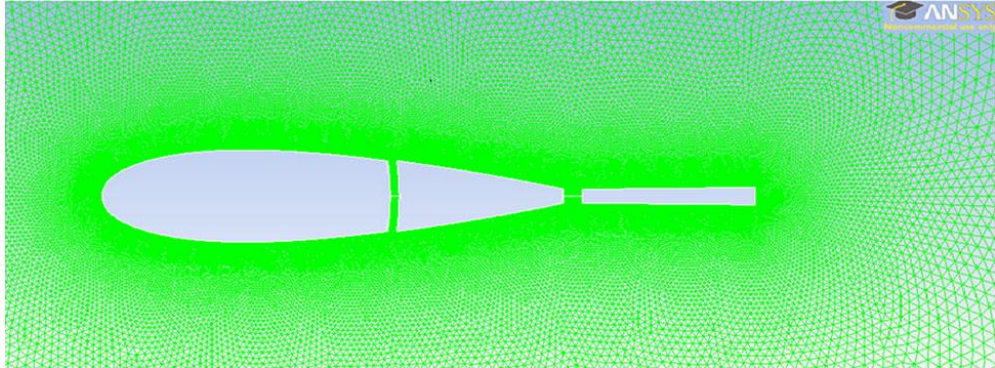


Figure 2.3 A multilink fish-based design vs an Ideal Body Wave

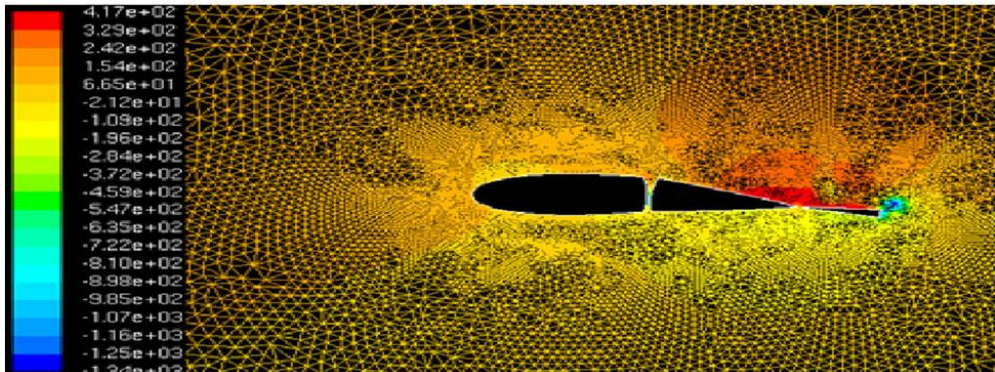
A method to obtain the parameters to replicate the body wave motion is to approximate it using a NACA airfoil for a given mode shape. Indeed, the NACA 0012 uses a symmetric aerodynamic profile that boosts the swimming speed while minimizing the drag, in a factor termed as swimming efficiency, for undulatory or oscillatory motion. Chowdhury et al. [14] investigated the effect of a NACA 0014 aerodynamic profile on a three link robotic fish using numerical simulations in ANSYS Fluent [14]. The simulations revealed that the controlling parameters of the fish motion and speed are the tail-beat frequency and the amplitude span of the tail tip. The results of their model are shown in Figure 2.4.

Furthermore, the numerical study in [14] showed that as the tail-beat frequency of a fish body is increased, both the positive drag (drag coefficient) and the negative drag (the propulsive force) are increased. It was concluded that an increase in frequency is directly proportional to the forward body speed and the size and velocity of the resulting wake for the tail beat. As the forward speed is increased, however, it is noted that the drag coefficient is increased until a certain level and then it decreases, forming a bell-shaped curve. This is only true for a certain operating range where the flow is laminar. Outside this operating range, the flow becomes chaotic and erratic. Therefore, it is recommended to maintain the flow around the tail tip to be under the turbulence limit. The amplitude span of the tail is another factor, which showed a high dependency

on the mode shape and maintained the effect seen by the tail beat frequency, i.e. the forward and lateral thrust on the fish body. The effect was shown as a bell shaped curve as the speed increased and the amplitude of the tail span increased and then gradually



(a) View of the 2D airfoil model mesh



(b) Coarse Unstructured Mesh in the far field regions away from the fish-body and Fine (tetrahedral) Mesh close to the fish-body

Figure 2.4 ANSYS simulations of the NACA airfoil being used for the aerodynamic profile [14]

decreased [14]. Thus, it was concluded that these two factors are the ones will be monitored closely while developing the design of the robotic fish.

2.1.4 Central pattern generation method of control: The central pattern generation method (CPG) uses a neural network to control the motion of each fin and tail end to accomplish a certain command function for the fish. Unlike BCF control, CPG requires the control of all fins to have an effect, including the pelvic, pectoral, caudal, and body fins to actuate motion. Therefore, each angle of the tail and individual fins is controlled independently in a harmonic fashion according to the equation shown below:

$$\theta_i = \bar{\theta}_i + A_i \sin(2\pi f_i t + \phi_i) \quad (i = 1, 2, \dots, N) \quad (3)$$

where θ_i denotes the angular position for the i th segment at time t , the $\bar{\theta}_i$ denotes the bias in asymmetric oscillations from the median, f_i is the frequency of the i^{th} segment, and ϕ_i is the phase difference of the sine wave in Equation (3 [1]. Other than allowing the designer parameterization of a complex swimming gait (i.e. lamprey or clown knife fish), it also enables to deal with faster control loops when compared to BCF, certain redundancies, and modulate movement using simplified commands [13]. The other advantage is that CPG method allows the neural network to control the motion of the fish body using its own learned weights and layers, which are the controlling factors within a common neural network. Neural network weights dictate how much a given input will impact the decision making while the layer network will dictate where that impact will be routed to. This enables the user to implement neural networks) and define a different architecture to suit their main purpose (favoring maneuverability over speed or vice versa) [13].

A typical CPG robotic fish model can be seen in the work by Yu et al. [13], which operates using a vision module, and the image is collected along with other sensory feeds. Other sensory feeds include but are not limited to: depth sensing, infrared sensing, IMU, gyro, accelerometer, and the encoder of motors to name a few. The collected image and sensory feed go into the motion control module, which houses the neural network. The neural network makes a decision on direction, speed, and whether or not to break from its set of weights. The control parameters of the motors (the hydrodynamic function for oscillatory amplitude denoted as Γ_i , the oscillatory frequency denoted as ω_i , and the bias in asymmetric oscillations from the median denoted as θ_i) are tuned in accordance to the sensory feedback and the motion control module's decision output. These are then feed into i^{th} version of Equation (3, and are mapped to their specific motors for a new motion. The new motion would then result in different sensory feedback which repeats the cycle. The neural network is programmed to move and tune certain individual fins for the required motion. For example, BCF forward swimming requires movement from the body and the tail, while sideward swimming requires the use of the pelvic fin. While this method is utilitarian when it comes to complex maneuvering and decision making, our design does not require that as of yet. The method has therefore been cast aside in favor of the less complex body wave control. The CPG method's utility in estimating the turning or

performing task beyond biomimetic movement is outside the scope of this thesis and as such is not used.

An equally significant factor in robotic fish motion is the method of actuation incorporated within its design. The method of actuation can determine the magnitude of forward propulsion, the overall size, and the types of lower level electronics implemented in the design.

2.2 Actuation Solutions

Approaches to robotic fish design mostly originate from the engineering research community. This is due to the fact that robotic fish offer some advantages in comparison to standard rotary propulsive mechanisms. For example, robotic fish, and bio-inspired vehicles in general, combine high efficiency over long distance travel as well as maneuverability at low speeds [15]. Furthermore, screw propellers, a common variant of rotatory propellers, are noted settle very slowly to thrust values that are small relative to its operating capacity[16]. Alternatively, researchers also construct robotic fish to verify hydrodynamic models in a free-swimming tank or in a static tail test. Regardless of objective, there is a wide corpus of robotic fish design in the literature [17]-[34]. While these designs are diverse, they can be categorized into two main groups based on their actuation mechanism.

1. **Motor-based actuation:** a motor or a series of motors are used to control a set of rigid links in a motion emulating the ideal body wave of their target species.
2. **Smart material actuation:** materials such as a shape memory polymer, Ionic polymer metal composites (IPMC), macro fiber composites (MFC), or a shape memory alloy (SMA) are used to actuate the tail.

2.2.1. Motor based fish designs The first robotic fish built by MIT was the RoboTuna in 1994 [35]. Its locomotion falls under the Thunniform, the category under which the tuna is classified. The purpose of building the RoboTuna was to explore better propulsion mechanisms for autonomous underwater vehicles.

The robot consists of an aluminum structure with 8 links in total (including body and fins) as displayed in Figure 2.5. The hull is covered with Lycra to prevent water ingress. The structure is actuated by 6 brushless DC motors. The robotic fish contains

multiple pressure sensors for both feedback and recording purposes. The robot was tested in MIT's free swimming tank, and the recorded data from the flow sensor at the tail tip were used as a variable in the closed loop control to optimize the motor angles and the swimming speed [35].

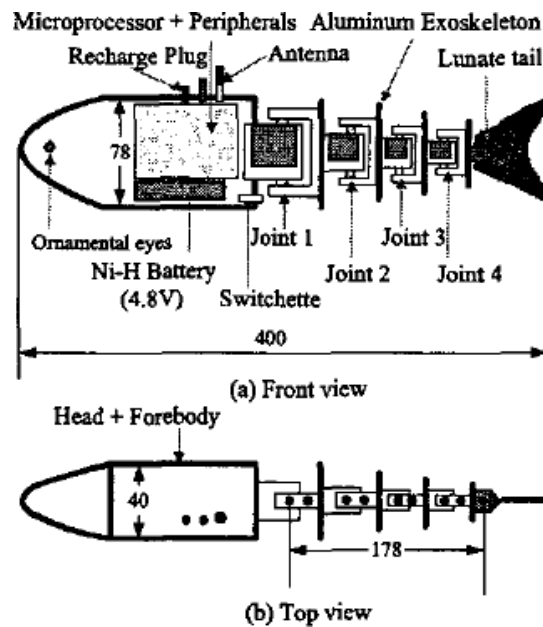


Figure 2.5 The Robotuna design schematic [34]

Zhang's Carangiform fish model attempted to replicate a fish body motion using a single motor for actuation [6]. It models the fish motion following Equation 1 for its ideal body wave and uses the estimated Strouhal number to design the TBF and AS of the robot to achieve the targeted forward velocity. The Strouhal number is a dimensionless number, which describes the oscillating flow mechanisms, and has a tie with propulsive efficiency in animals. The robot used the STM320 microcontroller unit to command the rotating angles of the fish, with the actuation mechanism shown in Figure 2.6. The transmission is perpetrated by the servo motor driving the input shaft connected to bevel gear 1, which consequently drives bevel gear 2. Bevel gear 2 drives the crank (labeled 3 in Figure 2.6) in a rotation which is connected to linkage 4, and finally resulting in the rocker actuating the tail in its intended motion. While Zhang's robotic fish body mimics that of a carangiform fish, the motion form is more akin to a simple oscillatory motion due to the fact only one joint is actuating the peduncle. Further explanation and justification can be found in section 3.1, which is titled "Ideal Body Wave Selection and Discretization".

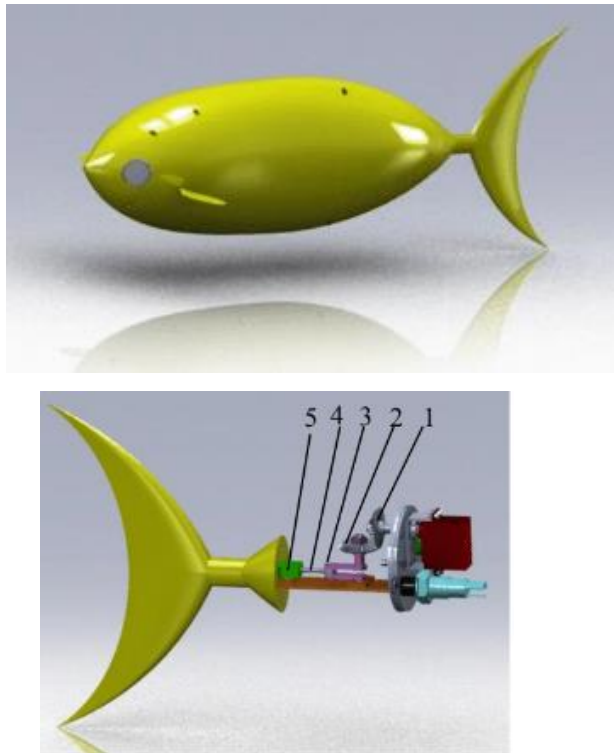


Figure 2.6 Zhang's Carangiform robotic fish CAD model [6]

An interesting take on the anguilliform locomotion was done by a team in the Virginia Polytechnic Institute and State University [36]. The robot was actuated by a series of 10 rigid links, whose motion body shifted from oscillatory to undulatory as it neared the tail tip from the body. The motor torques were calculated using the toolbox SimMechanics under MATLAB.

2.2.2 Smart materials based actuation While motor based solutions are relatively easily controlled due to the large corpus of literature surrounding their control schema, and possess a higher torque compared to other solutions, their large size makes them unsuited for certain applications. An alternative in this case is based on deploying smart materials, which are capable of actuating with minimal noise and act as a tail structure by themselves. This allows for stealthier designs, longer run times, and ease of space constraints for the designer.

As an example of smart materials, Ionic Polymer Metal Composites (IPMC) is an electroactive polymer-metal design which allows for large deformations with low applied voltages. This is due to the IPMC's structure, which consists of an anode layer

and a cathode layer. For instance, when a voltage of 2 V is applied from the anode to the cathode (as shown in Figure 2.8) [37], the cations are shifted to the cathode side while the anions are fixed on the carbon polymer chain. This causes a swelling on the cathode side and a subsequent shrinkage on the anode side, resulting in a bending motion.

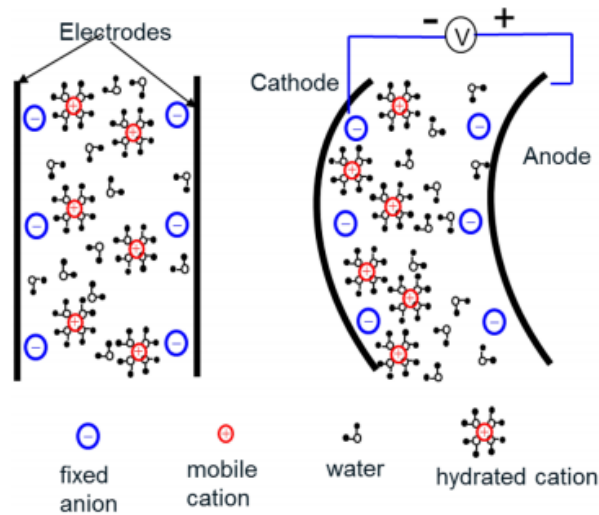


Figure 2.7 The actuation of an IPMC [37]

While relatively recent, IPMCs have been successfully used in robotic fish designs in the engineering research community. One such design was made by Tan’s group, whose motive behind choosing an IPMC for actuation is the collagenous structure of fish membranes [38]. Tan’s group successfully carried out experiments in a static tail and a free swimming testing apparatus. Tan’s team managed to maintain a speed of 0.125 BL/s (or 2 cm/s) at their optimal frequency where BL stands for body length.

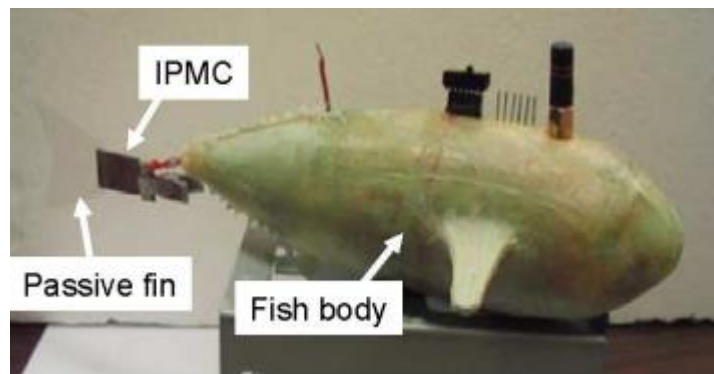


Figure 2.8 IPMC propelled robotic fish [38]

Macro Fiber Composites (MFC) are similar to IPMCs as they also perform a bending motion in response to a voltage stimulus, but they require a much higher voltage to operate than IPMC. In fact, some models require a voltage amplitude of at least 200 Volts to generate a significant bending stress and tip displacement. Erturk's team succeeded in actuating a finless robotic fish using an MFC operated at its resonance within quiescent water [39]. The team conducted two swimming tests, a static tail test and a free-swimming test, and concluded the robot's velocity to be 0.3 BL/s. Their model can be seen in Figure 2.10.

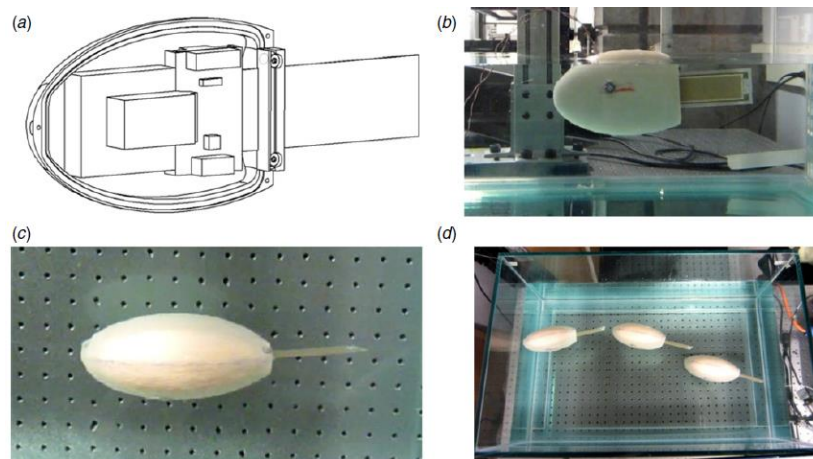


Figure 2.9 Untethered robotic fish actuated by MFC a) modeled view; (b) side view; (c) top view; and (d) combined motion capture with turning motion. Swimming speed when under actuation voltage of amplitude 1000 V at 5 Hz is approximately 7.5 cm/s [39]

2.3 Designs for Experimental Apparatus

The experimental apparatus for tail testing is divided into two different types, a static tail testing apparatus, where the tail is tethered and suspended at an observable level to the sensors around it, and a free swimming tank, where the robotic fish would swim freely under the observation of multiple sensors and high-speed camera to assess its swimming ability. While Static Tail tests are generally used for many vibrating mechanisms, the free-swimming tank is usually made in particular for underwater actuation. The static tail testing apparatus is used to quantify the tip position and forward thrust force of a robotic fish tail, while the free swimming tank tests the swimming performance directly by observing the robotic fish in the tank. Performance measurements in the swimming tank can include the forward speed, buoyancy, and ability to navigate an area in path planning. Multiple works show that the static tail test clamps the beam and suspends downward into an open tank under which it undulates (or oscillates) while being observed by a laser sensor or a vibrometer [37], [39], [40].

The measurements by the laser sensor are then recorded into a computer system where the tip position is analyzed against time. Thus, properties such as a robotic fish motion's speed, amplitude of undulation, and frequency may be analyzed.

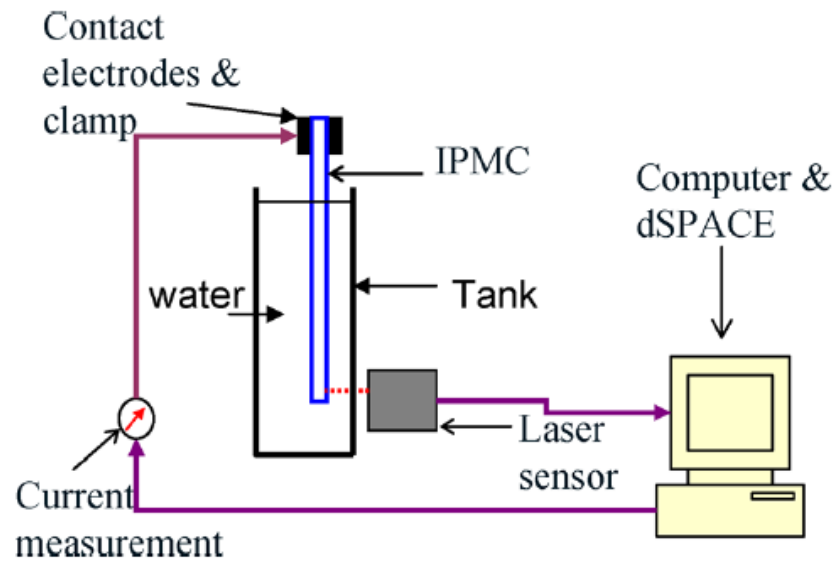


Figure 2.10 An example of a static tail testing apparatus [37]

Chapter 3. Methodology

In this chapter, the overarching methodology behind the robotic fish tail is explored. Robotic fish tails, and biomimetic structures in general, require a leveled methodology which transitions from the actual biology, to the simulated model, and finally to the actual robotic mechanism. To explore these stages with the necessary depth, this chapter is segregated as follows: The ideal body wave formulation and discretization section, the dynamic model of the robotic fish, the rigid body kinematics and control of the robotic fish.

3.1. Ideal Body Wave Selection and Discretization

This work is concerned with the biomimicry of various fish species, and the examination of whether or not fish properties of motion can be replicated in a robotic base. Therefore, we selected a list of three separate fish families to analyze with regards to their motion properties and swimming patterns. First, The fish families and species are selected and regarded in terms of their swimming ability and what their expected motion should yield at the end. Second, the selected fish species ideal body wave is formulated with regards to present literature. Third, this work's discretization method is explored, along with the final outputted results concerning the robotic structure.

3.1.1 Morphological selection In actuation morphology is the principle deciding factor in a fish's motion. While other biological factors may play some part in a fish's motion, it is morphology that is largely analyzed when creating a robotic fish. In the case of this thesis, the morphology of the fish's body movement will be examined. Thus, morphology will be the deciding factor used in this work to select the fish species. To best encompass the spectrum of BCF movements seen in figure 2.1, the Anguilliform (most undulatory), the Ostraciiform (most oscillatory), and Carangiform (an intermediate between undulatory and oscillatory), will be examined. In analyzing morphology, The following fish families will be examined:

- Carangidae, which has a carangiform motion
- Pholidae, which has an anguilliform motion
- Ostraciidae, which has an Ostraciiform motion.

3.1.1.1 Carangidae selection Carangidae are a fish family most noted to live in schools and travel great distances far from the coral reefs. As such, they are built for high speed forward swimming and little maneuvering [40]. Their motion form is named carangiform, which is exceptional amongst other fish types as it is noted to be the fastest and most efficient method of underwater motion. The carangiform method of locomotion entails the undulation of only the posterior half of the body with contracting waves [40]. Hence, it is predicted that the carangiform motion will perform the best out of all other selected fish families.

The selected species is the *Caranx sexfasciatus*, or the bigeye trevally. This species was selected due to its proximal habitat with UAE waters. The Big-eye trevally is a species that is found in almost all waters, and usually lives in large, albeit stationary, schools during the day. Despite this, it can cover large tracts of distance travelling as a group, allowing us more coverage of larger areas so that our observation is not limited to a set location. This species has a maximum reported length of 55 cm, its average size is usually within our design range.



Figure 3.1 A picture of the Bigeye Trevally in the wild [41]

Carangiform fish has an ideal body wave that can be approximated by a NACA airfoil profile. In this thesis, the symmetric NACA 0012 airfoil is considered as the ideal fish body in absence of the undulatory motion. The chord of the airfoil is taken as the fish-backbone which is assumed to undergo lateral deformation following a quadratic polynomial function multiplied by a sinusoidal wave [14], [42].

$$h(x, t) = \left(c_0 + c_1 \left(\frac{x}{l} \right) + c_2 \left(\frac{x}{l} \right)^2 \right) \cos \left(2\pi k \frac{x}{l} - 2\pi f t \right) \quad 0 \leq \frac{x}{l} \leq 1 \quad (4)$$

where x is the position along the streamwise direction, l is the length of the fish. The coefficients c_0 , c_1 , and c_2 are taken equal to 0.02, -0.0825, and 0.1625,

respectively, to simulate the kinematics of a steadily swimming carangiform fish [43]. k is the wave number and f denotes the frequency of the lateral oscillations, referred to as undulation frequency.

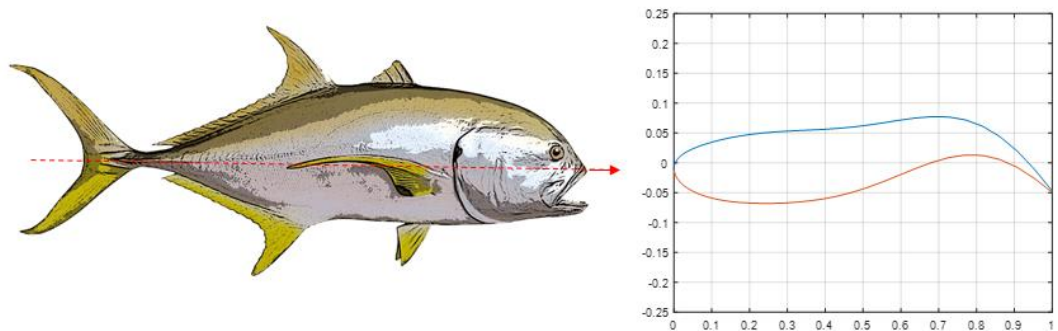


Figure 3.2 The ideal body wave of a bigeye trevally extracted

3.1.1.2 *Pholidae* selection The Pholidae family are a fish family that possess an eel-like appearance, have an elongated body with a small dorsal fin or no dorsal fin at all, and have the highest level of undulation amongst fish species [1], [4]. This type of movement is termed as anguilliform, where the body moves in a series of sinusoidal waves which cause each segment of the body to oscillate laterally across the axis of the body. Even though anguilliform fish motion often possess the highest angular amplitude with regards to their motion and a very high frequency of undulation, they are noted to have one of the slowest rates of forward propulsion. This can also be correlated to their habitat, which near shores and coral reefs where forward propulsion is not as important as maneuverability, an area which anguilliform locomotion excel at. As such, the anguilliform locomotion is predicted to be worse at forward speed than the carangiform but better at maneuvering than it.

The selected species is *Pholis gunnellus*, or the butterfish. This species was selected due to its exemplary snaking motion and its adaptability to robotic integration. This adaptability is due to the fact that the undulation of its tail can be managed with the proposed rigid links set which this work utilizes. The species itself is noted to live near the shorelines, and is noted to be a small burst swimmer. The species itself has some members which are 30 cm in length, but in the case of our work we will assume one that is the length of its Alaskan counterpart, the penpoint gunnel, which are known to reach 50 cm [44]. A NACA airfoil cannot be used to approximate the motion of a

butterfish without severe discrepancy between mathematical modelling and reality. As such, the following mathematical model is used to produce its motion [45].

$$h(x, t) = ae^{bx} \sin\left(\frac{2\pi}{\lambda}(x - Ct)\right) \quad (5)$$

where a denotes the head amplitude constant, set equal to 1.7 mm, b denotes the amplitude rise constant and is equal to 21.5 m^{-1} . λ is the wavelength (set equal to 0.096 m) and C denotes the wave speed (0.192 m/s). This model has been reported as a good approximation of butterfish motion [45].

3.1.1.3 Ostraciidae selection The Ostraciidae family are a fish family of small, bulky fish with a carapace protection around the body which allows for very minimal movement and as such little to no undulatory movement [46]. The Ostraciidae compensate for this by only oscillating their tail near the peduncle, which manifests a largely oscillatory motion, in a swimming motion termed Ostraciiform. This motion method is the opposite of other fish motion forms which utilizes large portions of their posterior body for undulatory movement. This type of movement also means that this fish family is notably slow and not particularly maneuverable, relying mostly on fins to move in a sway direction. As such, this fish family is likely to have the lowest mean forward thrust with regards to its motion.

The selected species is the *Ostracion cubicus*, or the boxfish. This species was selected due to its popularity in literature when modeling Ostraciiform locomotion. The boxfish, being a member of the *Ostraciidae* fish family performs a unique motion known as Ostraciiform. This swimming method utilizes only a single peduncle near the caudal fin to enforce propulsion, meaning that the ideal body wave in this case is stable with only the caudal fin oscillating at the end. As such, an ideal body wave motion cannot be used for the boxfish, as no such recorded ideal body wave exists to the best of our knowledge. This thesis instead utilizes the motion form of a previous work to encapsulate the boxfish's performance underwater [47], [48]. The motion of the boxfish is simply described by the following sine wave.

$$\theta(t) = A \sin(2\pi ft + \phi) \quad (6)$$

where A and f are the amplitude and frequency of oscillations. ϕ is the phase.

3.1.2 Ideal body wave discretization To mimic the fish species ideal body wave motion, a design scheme of the whole system is devised in such a way as to not compromise the biomimicry of the system or its engineered feasibility. As such, the robotic fish design utilizes a multi-rigid link structure, actuated by servo motors. This selection was made so that the thrust force can be maximized with a minimal voltage requirement. The design selection of rigid links rather than a flexible tail constrains the ability of emulating a fish's flexible profile to a complete manner, as the rigid links can never fully match the ideal body wave's curvature. This results in an area between the rigid link (termed $g(x)$) and the ideal body wave ($h(x, t)$) that is termed as an error in the biomimicry due to the rigid link method. The ideal body wave motion is discretized to an n number of rigid links. The number of links, n , dictate the manner of motion of the robotic fish as well as each motor's associated torque, angle, and motion frequency. The manner in which the link lengths were selected enables the design to minimize the area between the rigid links and the ideal body wave. This area is given by the following equation:

$$S_{sum} = \sum_{j=1}^3 \int_{Start_x}^{End_x} |h(x, t) - g(x)| \quad (7)$$

where $Start_x$ denotes the starting point of the link, End_x represents the end point of the link, $h(x, t)$ represents the ideal body wave curve, and $g(x)$ represents the rigid link represented as a function of x . The number of links n minimizes the S_{sum} value, which in turn indicates an improvement in biomimicry. This occurs due to the fact that the addition of more links increases the points of overlap between the rigid links $g(x)$ and the ideal body wave $h(x, t)$, which naturally increases the overlap between the rigid links and the ideal body wave, which in turn decreases the error area S_{sum} . The drawback to this approach is that an increase in the number of links can also result in under-sizing the motors, causing them to under-perform in the torque requirement area. Over multiple design iterations and in accordance to design recommendations found in literature [13], the n number of links was decided to be 3. This is not the only possible number of links for the robotic fish. It is, however, the design choice used in this thesis to best represent the species examined within its comparative analysis.

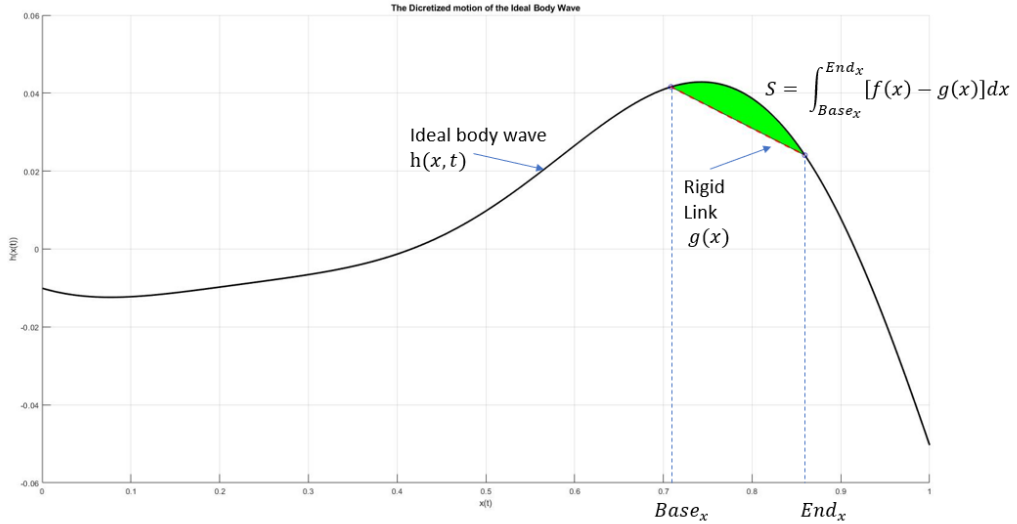


Figure 3.3 The discretization of the ideal body wave and a visual display of S_{sum}

The link lengths that best fit the bio-inspired solution are shown in Table 1. The optimization method used was done in a previous work where the ratios were obtained for separate cases of n number of links. The number of links recommended by Ruxu et al. in [1] recommend 3-4 links for carangiform and subcarangiform fish. Thus, the number of links n is used, the length of our design (further details in 4.1 The Robotic Fish Design), and the tabulated ratios from [49] to obtain the ratios that decrease the error area defined in Equation (7).

Table 3.1 The optimized Link Lengths

Link Number	Link Length in cm
1	13.5
2	9.72
3	8.77

The paramount endeavor in the discretization is obtaining the link motions and their respective angles, which would control the input to the motors and dictate the mathematical models and control scheme. To this end, we developed a discretization for the body wave as a function of time. The base of the robotic fish, and the beginning of the robotic tail, is selected to be at the middle of the body length to correspond to the carangiform design. All possible locations of the first link can be estimated using the equation below.

$$(x_i(t) - x_i(t)_{Base})^2 + (h_i(x, t) - h_i(x, t)_{Base})^2 = L_i^2 \quad i = 1, 2, 3 \quad (8)$$

The intersection of Equation 8 and in the ideal body wave equation dictates the end of the first link and the start of the second. Where $x_1(t)_{Base}$ and $h_1(x, t)_{Base}$ correspond to the base of the first link of the robotic tail in the x and $h(x, t)$ respectively. The method is then reiterated for each link, with each link's $h_1(x, t)_{Base}$ and $h(x, t)_{Base}$ corresponding to that of the previous iteration. A visualization of the process can be seen in the figure below:

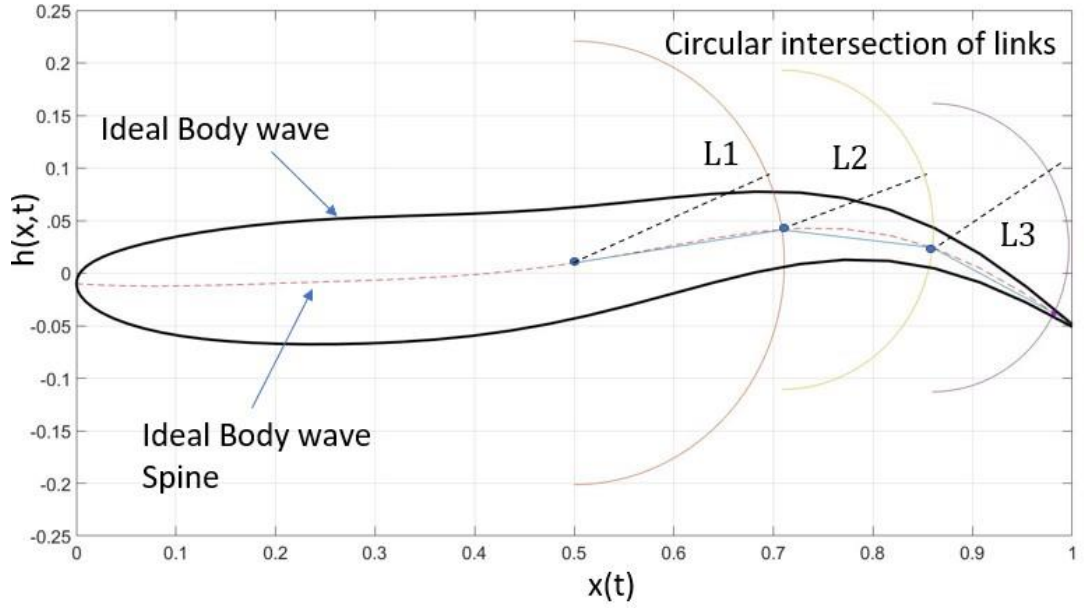


Figure 3.4 The discretization of the ideal body wave

The intersection of the circle defined in Equation 8 and the ideal body wave defined in Equation 4-5 (depending on the selected species) is found numerically. The resulting intersection points define $x_1(t)_{End}$ and $h_1(x, t)_{End}$, which denote the link end in the $x(t)$ and $h(x, t)$ axis, respectively. The link ends of L_1 would then define the base of the L_2 . Hence, it is concluded that $x_1(t)_{End} = x_2(t)_{Base}$ and $h_1(x, t)_{End} = h_2(x, t)_{Base}$. As such, Equation 8 can be reiterated for the second link and the third link in the same fashion. This method can also be used for a larger number of links, as it can be iterated over multiple times to best fit the ideal body wave. While a larger number of links is often preferable it entails some possible disadvantages. Said disadvantages include a high amount of voltage and current supplied to the motors and difficulty designing for servo motors that are significantly smaller than what can be found in market.

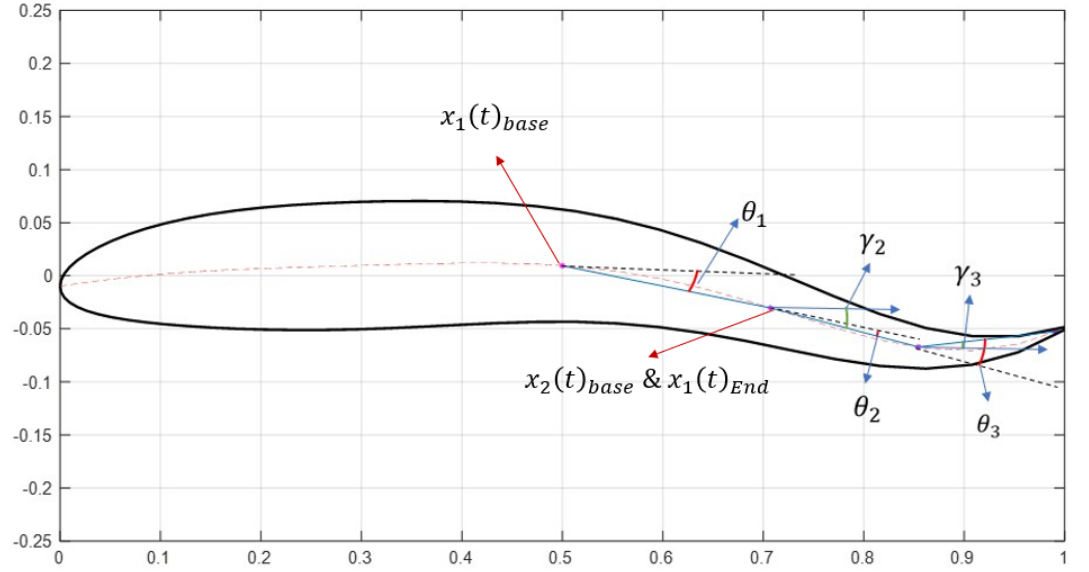


Figure 3.5 The numerical method of finding the fish motion visualized, where θ represents the angle relative to the previous link, and γ represents the absolute angle with respect to the global x-axis

The discretization method yields the positions of the beginning and end of each link in the robotic tail. Hence the angles needed to displace the tail in an approximation to the ideal body wave are obtained using Equation (9).

$$\gamma_i = \tan\left(\frac{x_i(t)_{End} - x_i(t)_{Base}}{y_i(t)_{End} - y_i(t)_{Base}}\right) \quad i = 1,2,3 \quad (9)$$

where i corresponds to the link number and γ_i is the angle of motion of a link i with respect to the global x-axis. The angles inputted to the servo motors are denoted as θ_i and can be computed from absolute angle γ_i in the following way:

θ_i corresponds to the relative angle of link i with respect to the previous link, $i - 1$. The angular positions can be utilized to obtain the discretized tip position for the robotic fish tail seen in Equation (8). The horizontal position of the tip of the tail is given by:

$$x_{tip}(t) = L_1 \cos(\gamma_1) + L_2 \cos(\gamma_2) + L_3 \cos(\gamma_3) \quad (10)$$

This position will be used to calculate the velocity of the tip, which is needed in estimating the induced thrust force.

The angles θ_i can be obtained from the absolute angles using a simple computation seen below, which can then be used as an input to the motors in the robotic fish.

$$\theta_1 = \gamma_1 \quad (11)$$

$$\theta_2 = \gamma_2 - \theta_1 \quad (12)$$

$$\theta_3 = \gamma_3 - \theta_1 - \theta_2 \quad (13)$$

3.2. The Robotic Fish Dynamic Model

The robotic fish's hydrodynamic model is designed as a means to predict the robotic fish's interaction with its environment. This is imperative as the robotic fish's interaction with its environment will dictate the necessary design considerations for the robotic fish and simulate its performance in underwater environs. It must also be noted that the robotic fish was not deployed into open waters as part of this thesis, which further necessitates a model to illustrate its potential performance underwater. This section will cover the robotic fish's dynamic model and the resulting PID tuning. First, the rigid body kinematics are explored, with a focus on obtaining the torques for each joint as a function of time. Second, the hydrodynamic effects imparted on the robotic fish are explored, with focus on the estimated thrust using a formulation technique. This formulation technique utilizes a combination of simulation and integration to obtain the forward thrust and speed of the robotic fish. Finally, the PID tuning is done for the resulting simulated torques.

3.2.1 Rigid body kinematics Hydrodynamic models can often be nontrivial in derivation. This is due to the fact an unconstrained marine body requires six degrees of freedom to fully describe its dynamics. Namely, these are the surge, sway, heave (representing the cartesian x-axis, y-axis, and z-axis respectively), and the roll, pitch, and yaw (representing the rotational axis in the x direction, y direction, and z direction, respectively).

In order to establish a similar frame of reference on the robotic fish, a diagram is built to observe the forward motion of each independently moving part. All segments are connected by revolute joints and to that end all segments are assigned their own rotational axis. In the case of this robotic fish design the center of gravity's z-axis aligns

with those of the revolute joints due to the orientation of the joints and the center of body's mass. As such the inertia frame F_g has axis (x_g, y_g, z_g) and an origin o_g .

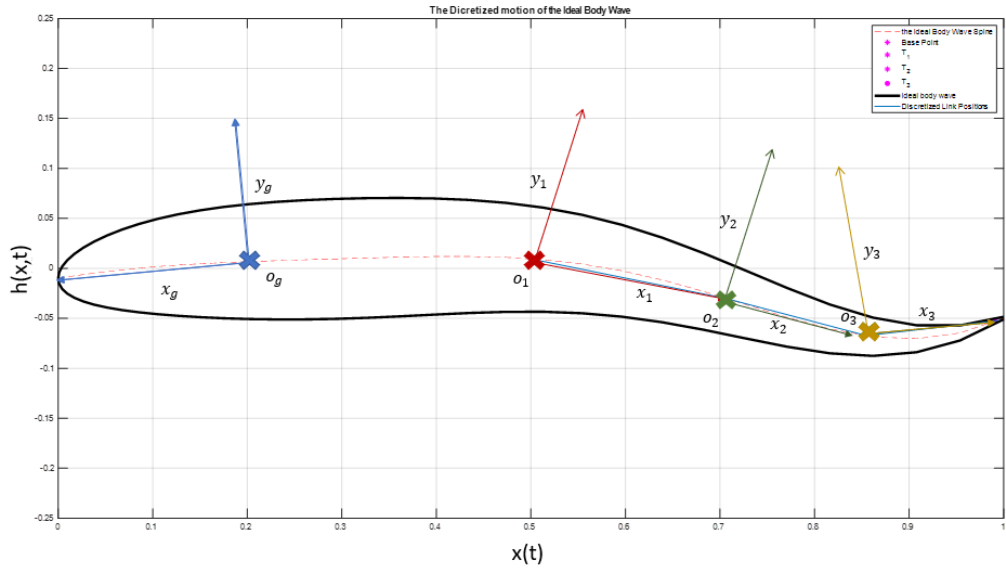


Figure 3.6 Coordinate frames of the discretized ideal body wave

It must be noted that the subscript label the different frames and where they are attached. As such, frames with a subscript g are the origin of the body's, subscript l denote the base of link 1, and so on. There are multiple ways to express the orientation of one frame with respect to another, such as quaternions, Euler angles, Gibbs vector, and others [50]. Due to the intuitive nature of Euler angles and its utility in representing orientations, this thesis utilizes it as a form of representation to construct the rotation matrix. To express the transformation relation between each frame, the right superscript is used. The rotation matrix between frames two and three, R_3^2 , represents the rotation of the third frame with respect to the second one. Thus, the expression of a rotation matrix between any two frames, i and j , with an XYZ rotation angles α, β, ϕ can be written as follows:

$$R_j^i = \begin{bmatrix} cac\beta & -sac\phi + cas\beta s\phi & sas\phi + cac\phi s\beta \\ sac\beta & -cac\phi + sas\beta s\phi & -cas\phi + sac\phi s\beta \\ -c\beta & c\beta s\phi & c\beta c\phi \end{bmatrix} \quad (14)$$

where α represents the yaw angle in the x-axis, β represents the pitch angle in the y-axis, the ϕ is the roll angle in the z-axis, and the c and s are abbreviations of cosine and sine. The position of the origin of frame j , with expressed in frame i is given as:

$$P^i = \begin{bmatrix} x^i \\ y^i \\ z^i \end{bmatrix} = R_j^i P^j \quad (15)$$

The rotation matrix can be utilized to obtain the angular velocity vector $\Omega_{i,j}^i$, between the frames i and j in terms of reference frame i .

$$\Omega_{i,j}^i = \begin{bmatrix} 0 \\ 0 \\ \theta_i \end{bmatrix} \quad (16)$$

A Simscape Multibody simulation is used to obtain both the linear velocity of each segment with respect to the global axis as well as the angular velocity vector $\Omega_{i,j}^i$. This is done using built-in blocks within the Simscape library and is expanded upon further in section 3.2.2 Thrust and forward speed models.

To represent the overall pose of the frames seen in Figure 3.6 (the position and the orientation of the frame), a transformation matrix is used. The transformation matrix of a frame can be represented as a combination of the rotation matrix and the position vector as follows:

$$T_j^i = \begin{bmatrix} R_j^i & P_j^i \\ 0_{3 \times 1} & 1 \end{bmatrix} \quad (17)$$

Thus, the pose between all frames shown in Figure 3.6 can be obtained using the transformation matrix seen in the equation above.

To represent the kinematic model of the fish tail, the robotic fish tail is considered to be a 3-linked planar robot, with three variables of motion corresponding to θ_i ($i = 1,3$). This robotic tail can be represented using a Denavit-Hartenberg table; shown in Table 3.2, which concludes the forward kinematics of motion of the fish tail and provides us with a standard representation of the model [51]. The $x(t)_{Base}$ and $h(x,t)_{Base}$ are taken to be a fixed origin of the system, with local coordinate centers are placed at each of the rotational joints. Therefore, there exists a local coordinate center at the end of each link. All joints rotate about the z-axis, which is perpendicular to the plane containing the fish. This system is represented as seen in Table 3.2. From this system, the forward kinematics are obtained, which relate the tail tip of the robotic fish with the base point of the tail.

Table 3.2 The DH parameters of the robotic fish

Joint/Frame Number	θ_j	d_j	a_j	α_j
1	θ_1	0	L_1	π
2	θ_2	0	L_2	0
3	θ_3	0	L_3	0

The utility of the DH parameter lies in its ability to construct transformation matrices between the consecutive frames based on the above parameters. The transformation matrix between frames i and $i - 1$ can thus be represented as follows:

$$T_i^{i-1} = \begin{bmatrix} c\theta_i & -s\theta_i & 0 & a_{i-1} \\ s\theta_i c\alpha_{i-1} & c\theta_i c\alpha_{i-1} & -s\alpha_{i-1} & -s\alpha_{i-1}d_i \\ s\theta_i s\alpha_{i-1} & c\theta_i s\alpha_{i-1} & c\alpha_{i-1} & c\alpha_{i-1}d_i \\ 0 & 0 & 0 & 1 \end{bmatrix} \quad (18)$$

The method used for controlling the angular position of the servo motors is a closed loop control method. The controller used in this work is the Proportional Integral Derivative (PID) controller. The present Dynamixel servo motors possess a built-in control architecture which utilizes a PID controller to achieve the desired motion. The control is applied as follows:

1. An instruction is given by the Microcontroller and is then registered as the goal position.
2. The goal position is converted to a desired position trajectory. The trajectory is transmitted as an input to the PID and feedforward controllers.
3. The Feedforward and PID controller calculate the PWM (pulse width modulation) output for the motor based on the desired trajectory.
4. The PWM passes through a limiter, which sets a limit based on the position trajectory.
5. The Final PWM value is given to the motor and the motor rotates, with the position recorded by the encoder
6. The encoder's measured position is compared against the desired position and is feed into the PID controller

A diagram of the PID's operation is shown Figure 3.7. The diagram encompasses the series of control instructions highlighted in the previous steps. The reduction in the diagram denotes the speed reduction mechanism in the motor, which allows for a higher level of torque by the servo motors.

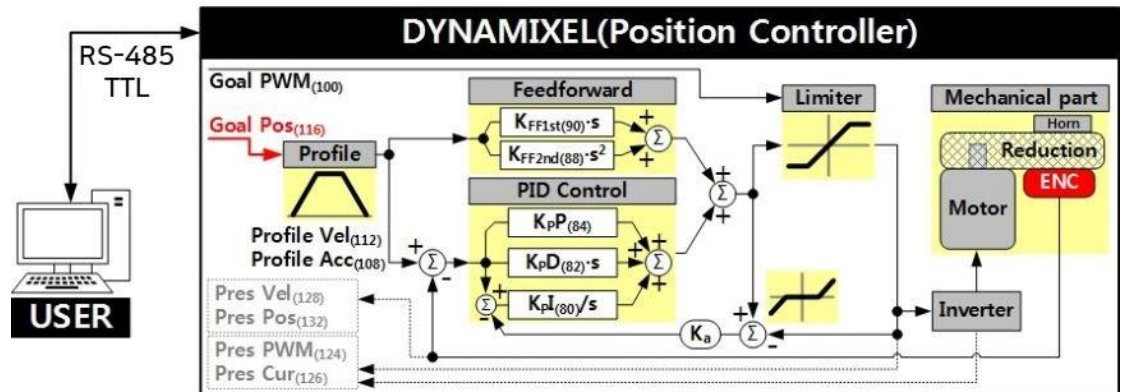


Figure 3.7 A diagram of the control architecture within the servo motors [52]

In this thesis, we only use a PD controller for the motion, with the integral gain being set to zero. The PD gains were obtained after a series of trial and error tuning and are given in Table 3.3.

Table 3.3 The PID gains for the dynamixel servo motors

Motor Number	Proportional Gain	Integral Gain	Derivative Gain
1	800	0	0
2	800	0	0
3	3000	0	250

The input angles obtained from the discretization method in section 3.1.2 are then compared with the actual angles obtained via the encoder reading. The encoder reading, in this case, is a 12-bit contactless absolute encoder. Absolute encoders are quite adept at position control scenarios due to their ability to record a unique position after receiving power. This, however, does not detract from their ability to track motion after being turned off. Optical and magnetic encoders are capable of giving a precise position value of the motor even after being turned off for a period of time, as each encoder position provides a unique reading. The error for the relative angles $[\theta_1, \theta_2, \theta_3]$ is 0.86%, 1.76%, and 4.25%, respectively, and can be seen in the figure below:

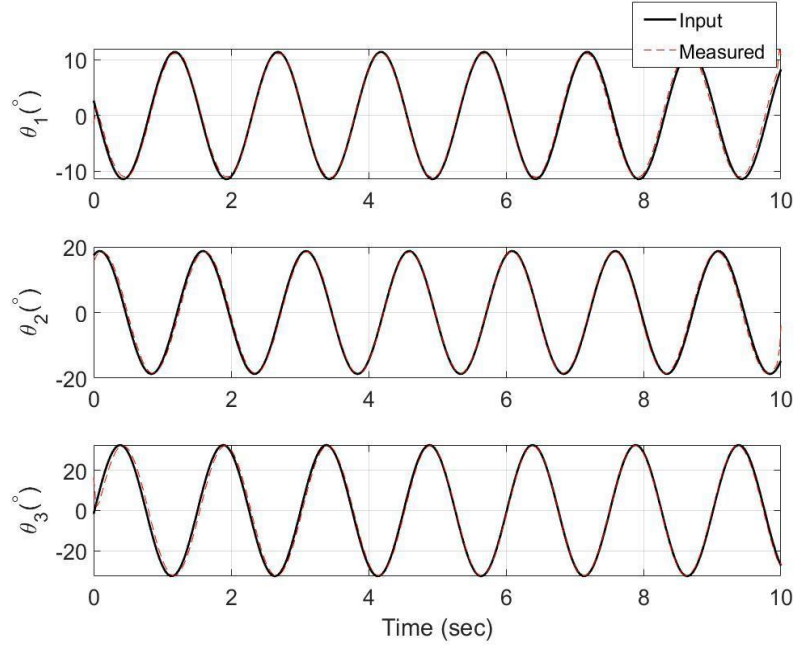


Figure 3.8 The input angles vs the output

To aid in the imitation of the robotic fish motion and verify the torques used in the PID tuning, a simulation was developed and compared with that of the ideal body deformation. The simulation was performed using the Simscape MultibodyTM simulation environment in MATLABTM. Simscape Multibody allows the user to simulate the mechanics of multibody objects in tandem with environmental effects from the prescribed motion. Therefore, the Coriolis forces, mass matrices, and Lagrangian force components are automatically computed based on the prescribed geometry. The internal damping and friction are incorporated within the internal mechanics of each joint. The drag force, however, is placed individually at each link segment using the computed force from the equation below.

$$F_{D_i} = \frac{1}{2} C_{D_i} \rho_w V_i^2 S_{A_i} \quad i = 1,2,3 \quad (19)$$

where V_i is the velocity, S_{A_i} is the surface area, and C_{D_i} is the drag coefficient of link i . The geometry is imported directly from Autodesk InventorTM (CAD diagram can be observed in section 4.1 The Robotic Fish Design) to ensure accurate representation of the system model. Figure 3.9 displays the sequence of the undulatory motion of the robotic produced by the articulated segments each actuated by a

servomotor. The results obtained from the Simscape simulator show the capability of the discretized model to reproduce the fish motion.

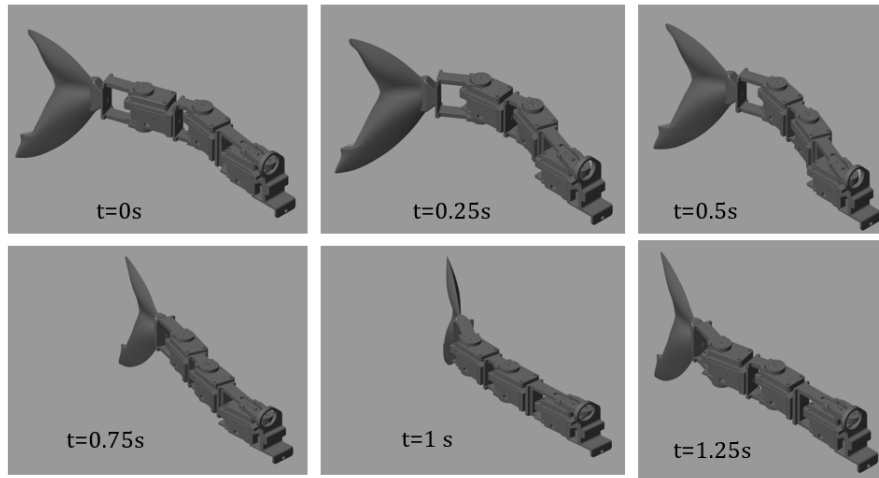


Figure 3.9 Undulatory motion of robotic fish: Simscape simulations.

The Simscape simulations were used to verify the optimized angle outputs with respect to the ideal body deformation. Such a comparison verifies that the optimized link lengths and discretization of the ideal body deformation match the biological reality that this work aims to approximate. The tip positions shown for the trajectory comparison are highlighted in Figure 4.1. The simulation is then used to draw a direct comparison between the tip locations and the ideal body deformation $h(x, t)$. The comparison between the analytical model and the Simscape Multibody simulations is displayed in Figure 3.10. The results are presented in terms of the trajectory of the tip of each articulated segment along the X - Y plane. The agreement between the obtained paths used in the following tests.

The trajectory path shows a fair match between the simulated path and the ideal body wave. This is especially true with the simulated path and the ideal body wave comparison between joints 1 and 2. The match wavers, however, at the highest tail beat amplitude for motor 3. This is due to the fact that the discretization method used favors matching the ideal body wave in terms of the entire wave rather than matching it only with the tip location. There is also the fact that the rigid links can never fully match the ideal body wave due to its inflexibility. Therefore, it is fair to conclude that this error will reappear in the results when matching the experimental motion of the robotic fish and the ideal body wave of the modeled species.

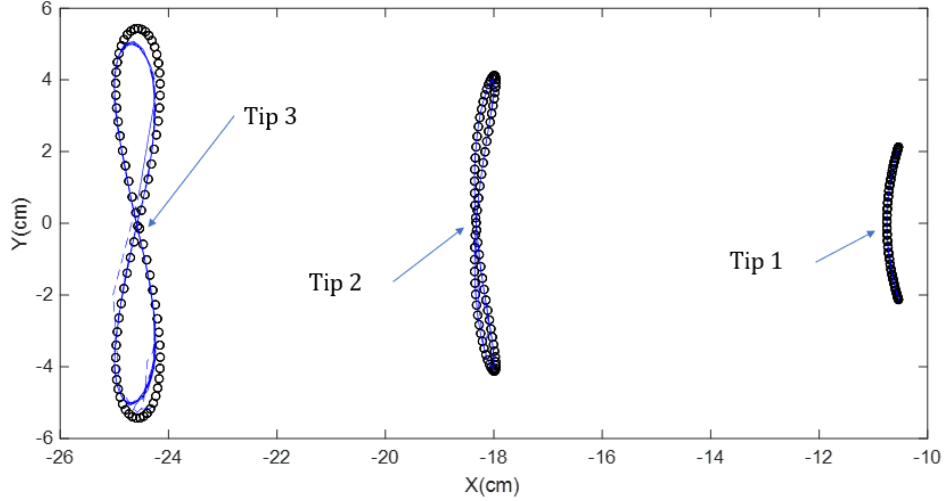


Figure 3.10 Tip trajectories: comparison between analytical model and Simscape Multibody. The X and Y coordinate system directly correspond to x and $h(x, t)$ as defined in Section 2

3.2.2 Thrust and forward speed models The robotic tail, bio-inspired by the fish species considered herein, possesses a varying cross-sectional area and can, as such, be defined as an elongated body [39]. Under that assumption, Lighthill's theory predicts that the mean thrust produced by the tail's motion, \bar{T} , is directly related to the tail's tip velocity and deflection and is given by [39]

$$\bar{T} = \left[\frac{m}{2} \left(\overline{\left(\frac{\partial h(x, t)}{\partial t} \right)^2} - U^2 \overline{\left(\frac{\partial h(x, t)}{\partial x} \right)^2} \right) \right]_{x=L} \quad (20)$$

where L is the total length of the posterior end and the overbar $\overline{(\cdot)}$ denotes the mean value. The virtual mass density at the tail tip, denoted by m is expressed as:

$$m = \frac{\pi \rho_w b^2}{4} \beta \quad (21)$$

where b denotes the base length of the posterior end including the caudal fin, ρ_w denotes the density of water, and β is the added mass coefficient which is assumed to be close to unity [53].

3.2.3 Robotic fish dynamic model Dynamic analysis of the robotic fish is performed in the inertial reference frame attached to the fish body and denoted by X , Y , and Z and a local frame represented by x , y , and z defined by the rotational angle as shown in Figure 3.11. The inertial coordinate system represents the fish body in terms of the world while the body-fixed coordinate system is attached to the fish body and its origin is the center of gravity of the body, denoted by C . θ and ψ denote the tail

deflection angle and the heading angle, respectively. The angle of attack is denoted by α . The velocity at point C is expressed in the body-fixed frame as $\vec{V}_C = (V_{cx}, V_{cy}, V_{cz})^T$. The induced actuation impacts the surge, sway and yaw motions represented by the velocity components V_{cx} and V_{cy} along the local x-axis and y-axis, and the angular velocity w_z around the z-axis. The corresponding forces include the net force in the x- and y-directions, F_x and F_y in the y-direction, and a moment M_z about the z-axis. Assuming that the three motion components are not coupled, the governing equations of the fish dynamics are written as [40], [54]:

$$(m_b - X_{am})\dot{V}_{cx} = (m_b - Y_{am})V_{cy}w_z + F_x \quad (22)$$

$$(m_b - Y_{am})\dot{V}_{cy} = -(m_b - X_{am})V_{cx}w_z + F_y \quad (23)$$

$$(J_{bz} - N_{am})\dot{w}_z = (Y_{am} - X_{am})V_{cx}V_{cy} + M_z \quad (24)$$

where m_b is the body mass, J_{bz} is the moment of inertia around the z-axis, N_{am} , Y_{am} , X_{am} are constant hydrodynamic constants that account for the added mass and are calculated based on an appropriately sized ellipsoid similar to that of the fish body. Their numerical values are given in Table 3.4. The net forces include the hydrodynamic induced forces by the posterior oscillations and forces on the moving robotic fish. They are expressed as [40], [54]:

$$F_x = F_{cx} - F_D \cos(\alpha) + F_L \sin(\alpha) \quad (25)$$

$$F_y = F_{cy} - F_D \sin(\alpha) - F_L \cos(\alpha) \quad (26)$$

$$M_z = M_{hz} + M_D \quad (27)$$

where the angle attack α is considered to be equal to zero in the present work. F_{cx} , F_{cy} and M_{hz} are respectively the hydrodynamic forces in the x- and y-direction and moment about the z-axis induced by the oscillating posterior, and F_D , F_L and M_D are respectively the drag and lift forces and moment acting on the body of the robotic fish as it moves. In the following, it is assumed that F_{cy} and M_{hz} are negligible to affect the overall steady state speed of the robotic fish in a significant way. The lift force F_L and moment M_D are assumed to be zero as the robotic fish tail is assumed to moving along the x-axis only. The drag force, F_D , is expressed in terms of the forward speed, the

surface area of the ellipsoid, S_A , is the density of the fluid, ρ_w , and the drag coefficient, C_D . C_D is taken to be that of an ellipsoid as 0.09 and the drag force is given by:

$$F_D = \frac{1}{2} C_D \rho_w V_{cx}^2 S_A \quad (28)$$

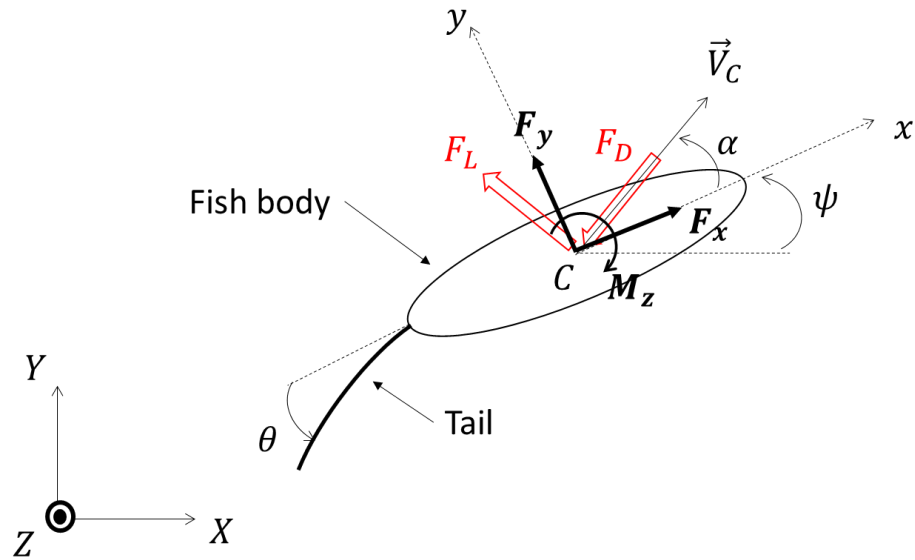


Figure 3.11 Representation of the hydrodynamic forces applied on the robotic fish (planar motion). Schematic adopted from [40], [54].

Table 3.4 Numerical values of hydrodynamic constants used in the estimate of the forward speed of the robotic fish obtained as a half streamline body from [40].

Hydrodynamic Constant	Value
X_{am}	-0.0621 kg
Y_{am}	-0.2299 kg
N_{am}	1.0413×10^{-4} kg m ²
J_{bz}	5.0797×10^{-4} kg m ²
C_D	0.09
S_A	0.0102 m ²
ρ_w	997 kg/m ³

Chapter 4. Experimental Setup

As stated previously in section 3.1. Ideal Body Wave Selection and Discretization, the biomimicry of a fish species through a rigid link robot is an intricate and nontrivial task. This is due to not only the optimization of the link lengths to match the species' ideal body wave, but also due to the control of the motors in the structure against hydrodynamic forces. This section discusses the construction of both the robotic fish and the experimental set-up used to test its performance. First, the robotic fish's design and construction are discussed in detail. Second, the experimental set-up's design, construction, measurement, and recording methods are discussed in detail.

4.1 The Robotic Fish Design

Whilst designing a robotic fish, a certain level of intricacy and robustness are required to bring the closest biological adaptation possible in a mechanized form. The link lengths calculated in the previous Chapter are built and constructed using a Stereolithographic 3D printer. The printer of choice, the ProJet 7000 HD, can print in precise detail due to its Stereolithographic printing material and its true line drawing in the X and Y axis [55]. The material used the Visijet M3 Crystal, possesses a density of 1.02 g/cm^3 , which is significantly lower than commercial PLAs and ensures the minimization of the servo motor torque requirement. This is also crucial to the biomimetic process, as a great degree of accuracy is necessary in capturing the motion of an ideal body wave using rigid link servo motors. The approximated model presented in this thesis should not deviate further from the ideal body wave, as that would risk a misrepresentation of the modelled species. A diagram of the robotic fish's CAD model is shown in Figure 4.1.

Another element of assurance in the attainment of a biomimetic robot is the responsiveness of the motors. The responsiveness of the motors will determine the degree of synchronicity between the motor angles and their ability to match the ideal body wave as a whole. To this end, Dynamixel XM-430-w350-t servo motors were selected. These servo motors each possess a built-in controller, which can be tuned in accordance to the PID values that best suit the required torque of the motors.

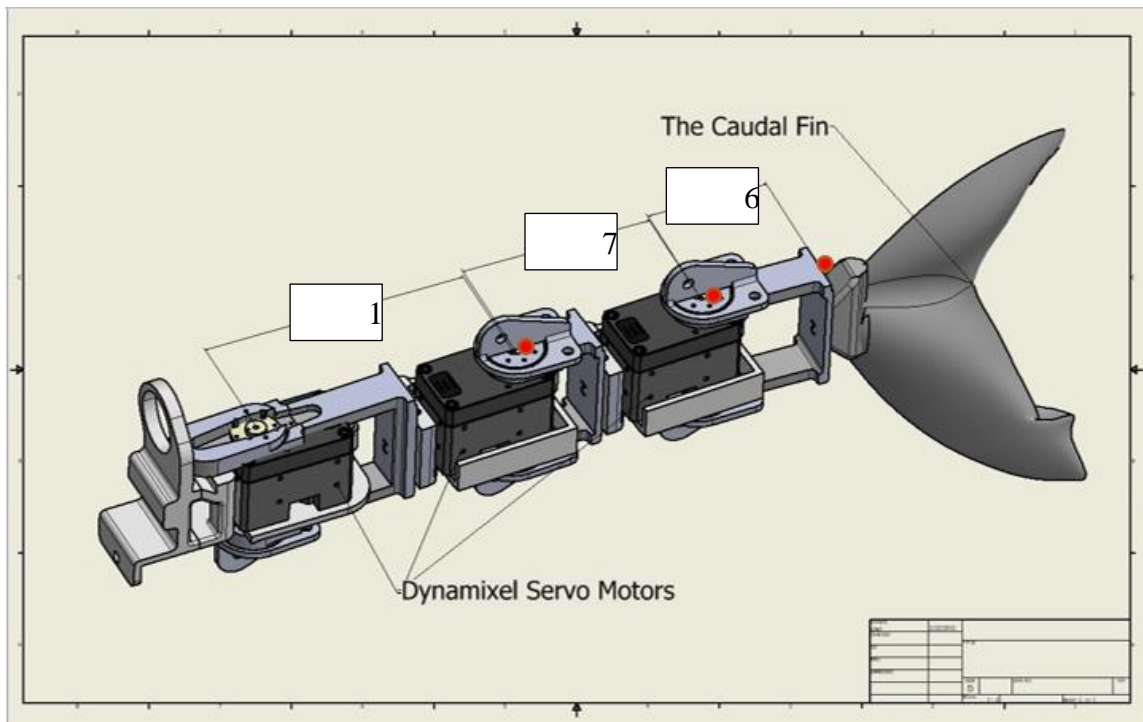


Figure 4.1 CAD model of the robotic fish

The PID values are programmed directly into the servo motors using a USB serial converter (dubbed by the company as usb2dynamixel). Each servo can have its own PID values in accordance to the position and torque requirement. The servo operation is routed through a main controller, the STM32F746ZGT6 based on a 32-bit ARM Cortex®-M7 with an FPU (floating point unit) operating at 216MHz, which communicates between the servo motors through a daisy chain on a set baudrate of 28800 symbols/sec, ensuring a rapid transmission rate. The water sealing is done using Religel from Hellerman-Tyton, which is a liquid material that can be poured into electrical compartments. The liquid solidifies after approximately 12 minutes, rendering the compartment with an IP 68 rating, which means that the robotic fish can be submerged underwater indefinitely. This also means that the robotic fish is dust proof, which while not applicable underwater, is an additional benefit to the waterproofing method's favor. The pouring and structuring was done using cover which protected the bottom motor.

A general design table can be seen below, where the major design elements seen for the robotic fish in this work are highlighted and summarized.

Table 4.1 A general design table for the robotic fish

Link 1	Link 2	Link 3	Material	Sealing material	Servo motors	Caudal fin width	Total mass
107.52 mm	77.56 mm	67.46 mm	Visijet M3 Crystal	Hellerman-Tyton's Religel	XM-430-w350-t	188.6 mm	1.1876 kg

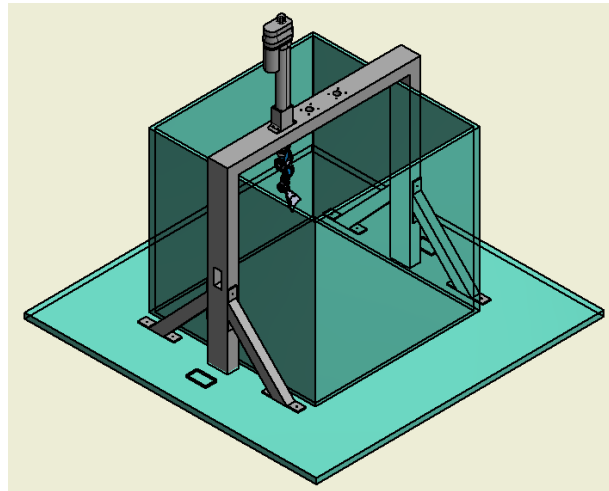
4.2 The Experimental Set-up Design

The evaluation of the robotic fish tail's swimming performance necessitates the development of a testing platform. The testing platform was built to measure and record the tail tip position and the generated thrust of the robotic fish tail. The laboratory set up was designed to ensure that a robotic fish tail's position can be recorded at multiple points along the tail. This also ensures that the set up is flexible enough to test on other robotic fish tails in future works. This is performed using a linear actuator which moves the tail vertically, allowing the laser to read the tail tip position at the desired vertical location. The linear actuator comes with an added advantage of allowing the set-up to adapt to a variety of tail lengths, which allowed for remarkable flexibility in design during the early stages of the robotic fish development. The position measurements were conducted using a *BaumerTM* OM70 laser point sensor, which transmits measurements via a voltage signal indicative of the displacement the robotic tail.

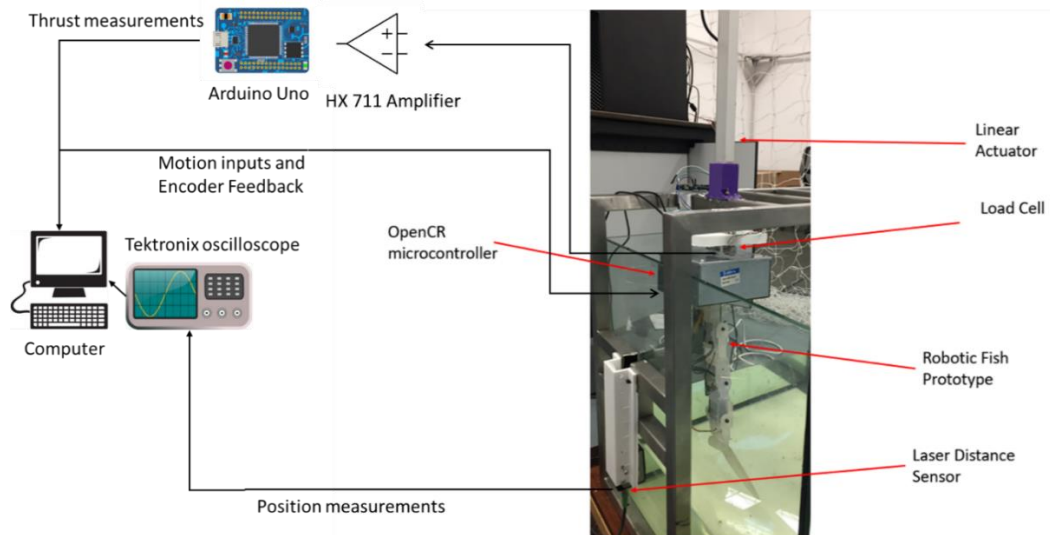
The displacement is mapped over time using a *TektronixTM* TDS 1002B oscilloscope, which measures the displacement of the tail over a 25-second interval. The data obtained through the oscilloscope is transferred to MATLAB using a customized script, where it is recorded and catalogued. The customized script automatically numerates the data and logs it into a folder which allows for easier review later on. A similar script is also utilized for the load cell measurements.

It is important to note that robotic fish's main thrust contribution occurs at the tip of the caudal fin [6], and as such all position measurements involving the laser sensor are allocated upon the tip of the caudal fin. The original proposed CAD design and the

actual laboratory set-up are displayed in Figures Figure 4.2(a) and Figure 4.2(b), respectively.



(a) CAD model (initial design)



(b) Actual set-up

Figure 4.2 The experimental set up

This work is primarily concerned with the measurement of underwater thrust. The thrust measurements were obtained via a load cell suspended vertically above the tail. The load cell was placed in such a way that the robotic fish's forward propulsion would enforce a bending moment upon it, which results in a forward thrust measurement. The load cell was also placed in such a way that the sideways reaction force due the oscillation of the robotic fish within water is reduced due to the fact that the force would then translate as a torsion upon the load cell, which is a minimal effect in the measurement in comparison to a bending moment. Any sway force F_{c2} on the load cell

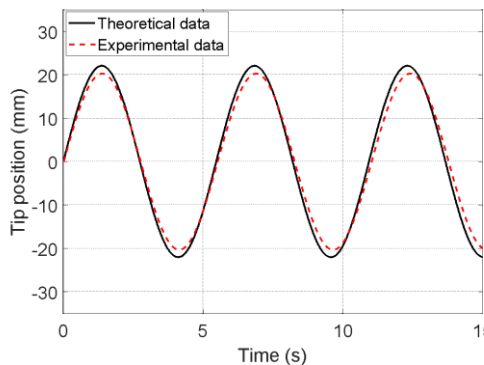
has a minimal effect, which serves our purposes as the effect of the forward thrust, F_c , is the primary focus in this thesis. The load cell was calibrated using a set of standardized weights of 6.5 and 4 grams on separate cycles. This was carried out to find the calibration factor of the load cell and to ensure that the load cell arrangement performs as expected against upward thrust. The calibration factor is stated by the manufacturer to be unique to each load cell and then it was found through a series of trials using the standardized weights. The load cell output voltage changes were amplified through an HX-711 Amplifier, which communicates serially with an Arduino Uno. The Arduino then transmits the thrust measurements at a rate of 10 Hz before the data is recorded and catalogued through a customized MATLAB script.

Chapter 5. Results and Analysis

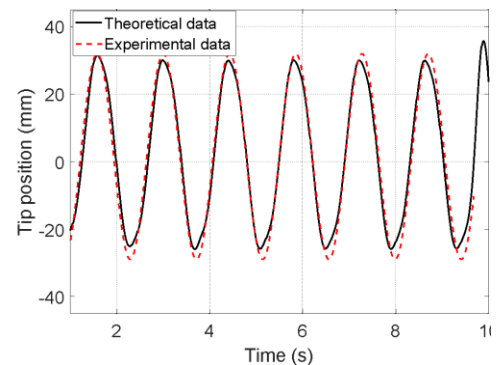
In the analysis of the experimental data, the observed deformation of the robotic fish posterior is first compared to that of the original ideal body deformations of the considered fish species. Secondly, the thrust is measured over a range of frequencies and angular amplitudes and compared to Lighthill's theory. The comparison is semi-empirical, meaning that the motion from the laser sensor measurement was used to compute the Lighthill's formula. Consequently, the forward speed of the aforementioned range of frequencies and angular amplitudes is obtained from the numerical integration of Equations (22)-(24). Finally, the three fish families (Trevally, Butterfish, and Boxfish) are examined at their discretized angles to while measuring their thrust force and thereby their cruising speed. The cruising speed of each fish family is then compared to previous robotic fish works in terms of body length and forward speed.

5.1. Experimental Verification

A comparison between the measured displacement of the robotic fish tail tip and the associated displacement in an ideal body deformation is shown in Figure 5.1. The results are presented for different undulation frequencies. Clearly, the robotic fish exhibits the same frequency as that of the ideal body deformation. The errors are noted mostly at the displacement peaks, where the error is within 2.58% with respect to the ideal body deformation. These errors are the result of delayed settling time of the PID controller, and can be adjusted in future works.



(a) $f = 0.225$ Hz



(b) $f = 0.55$ Hz

Figure 5.1 Time variations of the caudal fin position: measurements vs. analytical model. Results are shown for two different undulation frequencies.

Before proceeding with the performance analysis of the robotic fish tail, the implementation of the load cell must first be verified. This is done to ensure that the data obtained is an accurate measurement of the thrust generated by the robotic fish tail. Different oscillatory motions, with varying the frequency and amplitude of the actuation angle θ_3 of the third servomotor, are done on the robotic fish tail. The other angles θ_1 and θ_2 are set to zero. The experimental results along with those obtained from Lighthill's theory are shown in Figure 5.2. The frequency range has a constant angle amplitude of 30 degrees while the amplitude range has a frequency of 0.55 Hz across all recorded values. The results are in good agreement with their theoretical counterparts. This validation was done so that an equivalence between the mean of the Lighthill's theoretical model (Equation (20)) and the experimental observation of the mean of the thrust force of the robotic fish is established. It must be noted that the Lighthill's model is implemented with empirical data of the tail motion. The tail tip speed component, denoted as $\left. \frac{dh(x,t)}{dt} \right|_{x=L}$ in Equation (20), is obtained through the time derivative of the tail tip position measurements obtained from the laser sensor. The experiments are repeated 3-4 times to verify the consistency of the thrust measurements. As shown in Figure 5.2, the thrust increases with the increase in frequency and amplitude, which is consistent with Lighthill's theory. It should be noted, however, that a significant difference occurs when the frequency reaches 0.65 Hz. This is mostly due to the fact that the swaying force reaches high values at that point and/or the impact of the tail's width, which causes amplification of the side forces generated at higher frequencies. In this work, the focus is the study of the thrust force production while neglecting the effects of the swaying force or reactionary forces due to the tail's flapping motion. Therefore, the frequency variation will be limited to the range reported in Figure 5.2(a). Regardless of outliers observed at high values of the frequency, the experimental results obtained when varying the frequency and amplitude of the actuation angle indicate that the robotic fish tail's performance, in terms of mean thrust, is consistent with Lighthill's theory and demonstrates the capability of the experimental set-up to analyze the swimming performance of different bio-inspired propulsion mechanisms. Thus, the comparative swimming analysis of the various fish species can be done with a degree of verification based on the match between the lighthill theory and the experimental results.

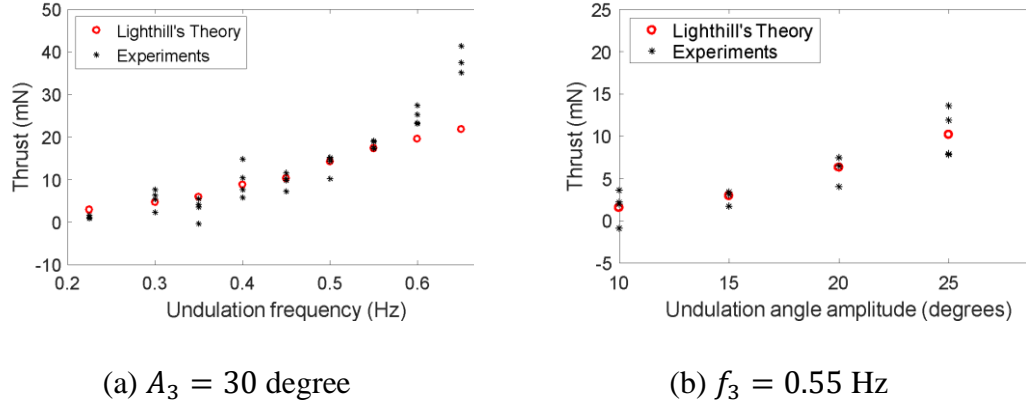


Figure 5.2 Variations of the mean thrust with the undulation (a) frequency and (b) angle amplitude: experiments vs. Lighthill's theory.

The mean value of the thrust is then utilized to obtain an estimate of the forward speed for the robotic fish tail. While the hydrodynamic constants are contingent upon experimentation and further fish body design, they were selected to provide enough of an equivalence with respect to previous works reported in the literature [56], [57]. Thus, Equations (25)-(27) were numerically integrated to obtain the forward speed using the mean thrust values from Figure 5.2. The resulting forward speed obtained over the range of frequency and amplitudes of the actuation angle θ_3 of the third servomotor are displayed in Figure 5.3. The forward speed exhibits quadratic increase with increasing frequency and amplitude of the angle.

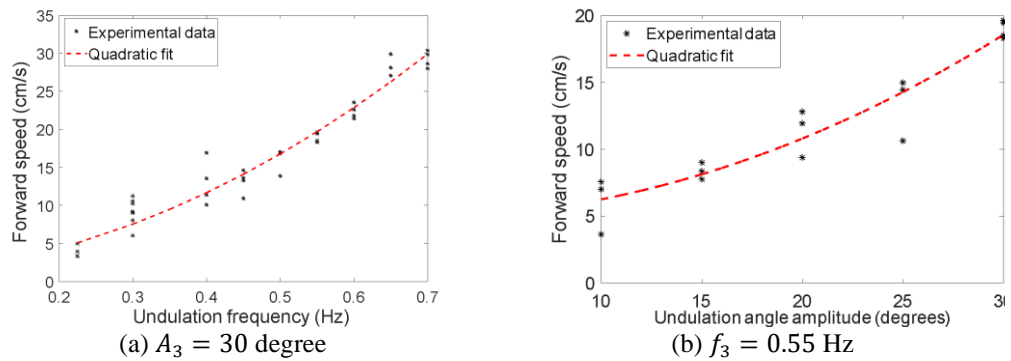


Figure 5.3 Variations of the mean forward speed with the undulation (a) frequency and (b) angle amplitude.

5.2. Comparative Swimming Performance Analysis

The primary objective of this work is the comparison of the performance of robotic fish based on different fish species in terms of motion and hydrodynamic propulsion. The genetic variety between the three species, which belong to separate fish families, manifests itself in both their morphology and motion forms. A comparative image of

the locomotion of the three fish species is shown in Figure 5.4. This figure reveals the morphology of the fish species resulting in different swimming characteristics in terms of undulatory frequency and tail lateral displacement. The three fish species difference in locomotion waveforms carries over through the discretized methods to obtain the angular inputs of the servomotors. Then, the testing platform is used to examine the swimming performance of each robotic fish.

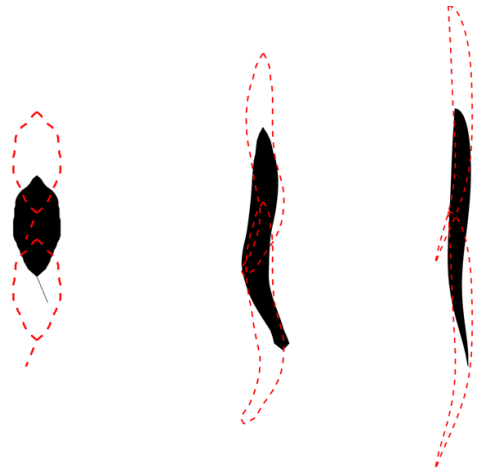


Figure 5.4 Locomotion of three fishes under investigation from left to right boxfish, butterflyfish, and trevally.

The motion of each fish is obtained through the previously mentioned ideal body waves and experiments are conducted to obtain the thrust measurements and estimate their forward speed. We present in Error! Reference source not found. the characteristics and swimming performance of the three fish models. The transient variations of the thrust are presented in Figure 5.5. The boxfish has a nearly sinusoidal thrust force because only the third servomotor is mimicking the motion of the caudal fin as opposed to the collective entirety of the servos working in synchronicity to mimic the ideal body deformation as in the other two species. Clearly, the boxfish model is predictably the slowest of the three species, with a mean thrust of 6.46 mN. This also reflects the reality that the boxfish is a reef fish and best suited for tight maneuvering and bursts of speed rather than long journeys at sustained cruising speed [47].

The butterflyfish possesses the most undulatory motion of the three fish species considered herein, due to it being a member of *Pholidae* family, which are eel-like in appearance and live within coral reefs [58]. The motion form of the butterflyfish is termed as anguilliform, and possesses the largest angular amplitudes compared to the other

motion forms. This also mean that the angles combine in synchronicity not to increase the forward thrust motion but to increase the maneuverability of the butterflyfish motion [1]. The plots in Figure 5.5(b) show that the butterflyfish is the second fastest fish in terms of mean thrust, despite possessing the highest maximum thrust recorded and the lowest minimum thrust recorded. The butterflyfish's mean thrust is found equal to 19.81 mN yielding an average forward speed of 20.7 cm/s.

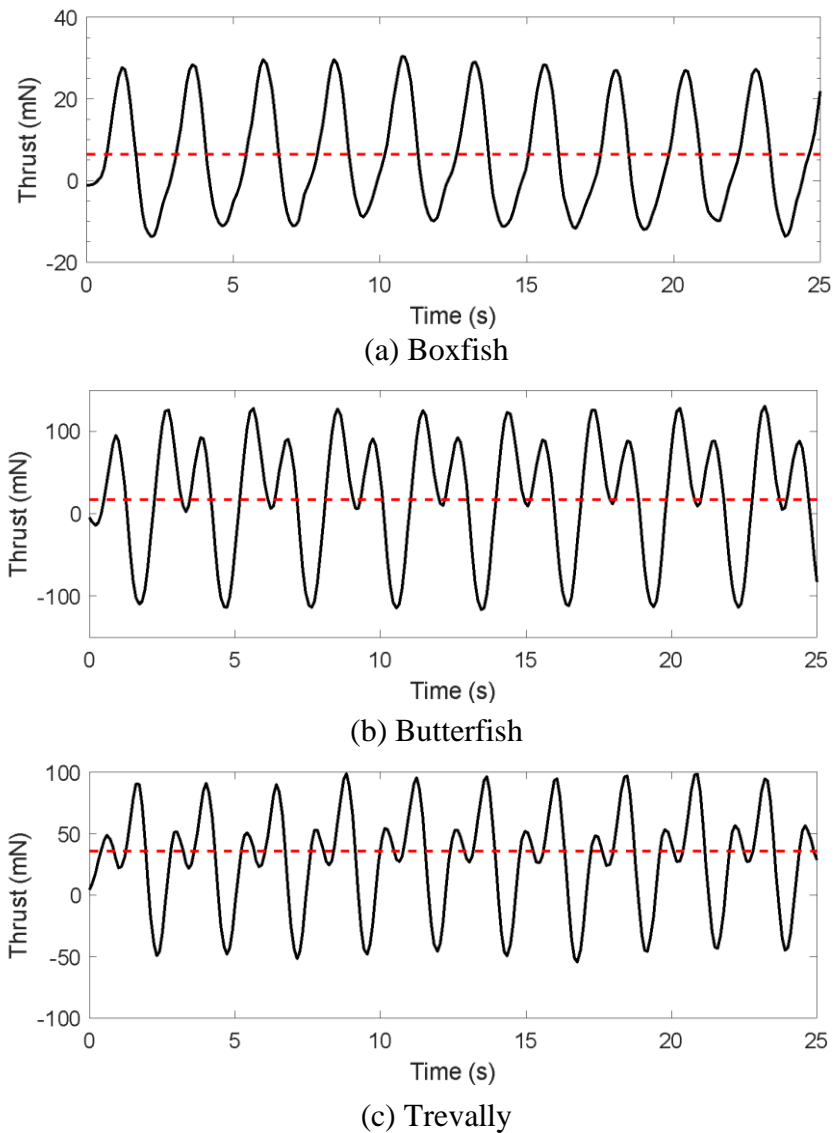


Figure 5.5 Time variations of the thrust of the three fish models: (a) boxfish, (b) butterflyfish, and (c) trevally. Dashed line indicates the mean value of the thrust.

The big-eye trevally is the fastest of the three species, due to it being a member of the *Carangidae* family. The *Carangidae* family excel in long distance by the capability to generate high cruising speed [41], [59]. This is especially true of the big-eye trevally, which moves as a part of a larger school over long distances. While it does not have as

high of angular amplitude as the butterflyfish, the big-eye trevally exhibits a synchronicity of angles that allow it to generate a higher mean thrust with a value of 29.8 mN that results in the highest forward speed of 25.2 cm/s.

One common metric used to compare the performance of robotic fish is the ratio of the body length to the forward speed, BL/s. To illustrate the position of the present work in comparison to other robotic fish studies using different propulsion mechanisms, a performance comparison chart is presented in Figure 5.6. The comparison chart contains results from previous studies that made use of different actuation methods to achieve specific design objectives. Notably, smart materials such as IPMC, MFC, and SMA resulted in slower robots when compared to their motorized counterparts. Although, these smart materials can generate higher vibration frequencies than their motorized counterparts, they lack the capability to generate the required torque to induce large amplitudes motions, which are needed for high forward speeds. While this work does not encompass the design of a robotic fish body, it is possible to hypothesize a distinct robotic fish body design and size based on the species listed previously. The chart shows that this robotic fish tail performs adequately when compared to previous works, averaging slightly less than robotic fish in the 60 cm and above category while performing similarly in comparison with smaller fish types. The robotic fish tail's best performance occurs when modelled using the big-eye trevally due to its highest forward speed of all three species. A possible improvement that can be done in future works is a free-swimming experiment where the species are modeled at higher frequencies.

Table 5.1 Swimming performance of the three fish models.

	Boxfish	Butterfish	Trevally
Amplitude of undulation angles in degrees ($\theta_1, \theta_2, \theta_3$)	(0°,0°,20°)	(20°,30°,35°)	(17.6°,17°,39°)
Phase of angles in degrees ($\theta_1, \theta_2, \theta_3$)	(0°,0°,0°)	(-44°, -44°, -35°)	(-23°, -35°, -30°)
Frequency (Hz)	0.55	0.5	0.75
Mean thrust (mN)	6.46	19.81	29.8
Max and min of thrust (mN)	(11,30.3)	(-173,170)	(-49.41, 98.64)
Forward speed (cm/s)	10.2	20.7	25.2

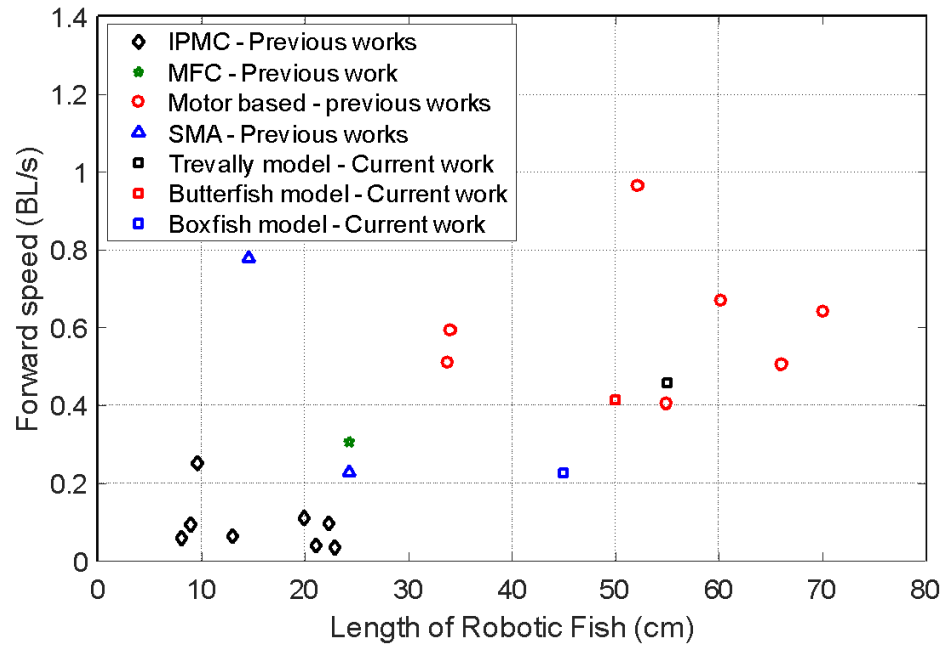


Figure 5.6 Forward speed vs. length of robotic fish length: comparison against previous studies reported in the literature [57], [60], [69]–[78], [61]–[68].

Chapter 6. Conclusion and Future Work

In this Thesis, we presented an analysis of the performance of three fish species, modeled as robotic fish. The ideal body wave was attained for the three species through a variety of methods, starting with a biological approximation for the big-eye trevally, a mathematical model of fish movement for the butterflyfish, and an observation of previous works for the boxfish. The ideal body waves were then discretized in combination with a series of optimized link lengths. This work developed a robotic fish tail capable of mimicking three types of propulsion systems. A rigid body dynamic model was developed using Simmechanics to analyze the torques placed on the motors and was later used to tune the PID for the associated motors. A hydrodynamic model based on Lighthill's theory of elongated bodies was also implemented to compute the thrust generated by the motion of the tail and estimate the forward speed of the robotic fish. The tail was 3D printed and servomotors were deployed to actuate the system. The robotic fish tail was then examined against the ideal body wave and was found to match with it with a maximum error of 2.58%. A testing set up was also developed to measure the generated thrust and tip displacement of the robotic fish tail, which utilized a laser sensor and an amplified load cell to acquire all needed measurements. The thrust was then obtained over a range of frequencies and amplitudes of the actuation angle. The experimental results showed a good agreement with Lighthill's theory of elongated-body propulsion. Finally, the swimming performance of three fish species were examined in terms of thrust generation and forward speed. A set of experiments was conducted to reproduce the biological features in the undulatory (or oscillatory) motion for each fish. The trevally was found to produce the fastest swimming with an estimated forward speed of 25.2 cm/s. The experimental results were also compared to previous studies on robotic fish reported in the literature.

As for future work, the developed testing setup can be used to analyze the tip position and propulsion of multiple kinds of robotic fish, e.g., deploying tail made of smart materials such as MFC and IPMC. Moreover, the setup can be deployed to analyze a variety of propulsion methods, from standard screw propellers to squid-inspired thrusters. The hydrodynamic model developed in this work can be used for a path-planning algorithm for a robotic fish, an area that is not explored often due to the

complexity of fish underwater propulsion. The hydrodynamic model can also be used to analyze different fish species in terms of maneuverability rather than forward propulsion, which could lead to the development of different path-planning methods for underwater propulsion using biomimetic robots. A possible extension of the current work can include the implementation of the full robotic fish and conducting a free-swimming test. In this test, a high-speed camera will be deployed to track the swimming path of the robot. The latter will be equipped by a wireless module, which receives commands from a computer and transfers them to the microcontroller to operate the motor as per the needed actuation. The robot components need to be carefully placed inside a waterproof enclosure (streamlined body) so that its center of gravity is located below the center of buoyancy to ensure the longitudinal and transverse stability and obtain neutrally buoyant robot.

References

- [1] R. Du, Z. Li, K. Youcef-Toumi, and P. V. y Alvarado, *Robot fish: bio-inspired fishlike underwater robots*. London: Springer, 2015.
- [2] A. Raj and A. Thakur, “Fish-inspired robots: design, sensing, actuation, and autonomy—a review of research,” *Bioinspir. Biomim.*, vol. 11, p. 31001, 2016, doi: 10.1088/1748-3190/11/3/031001.
- [3] W.-S. Chu, K.-T. Lee, S.-H. Song, M.-W. Han, J.-Y. Lee, H.-S. Kim, M.-S. Kim, Y.-J. Park, K.-J. Cho, and S.-H. Ahn, “Review of biomimetic underwater robots using smart actuators,” *Int. J. Precis. Eng. Manuf.*, vol. 13, no. 7, pp. 1281–1292, 2012.
- [4] C. M. Breder Jr, “The locomotion of fishes,” *Zoologica*, vol. 4, pp. 159–291, 1926.
- [5] M. Sfakiotakis, D. M. Lane, and J. B. C. Davies, “Review of fish swimming modes for aquatic locomotion,” *IEEE J. Ocean. Eng.*, vol. 24, no. 2, pp. 237–252, 1999.
- [6] R. Zhang and H. Zhang, “Simulation and Analysis for Propulsion Mechanism of Carangiform Robotic Fish on ADAMS,” in *2018 IEEE International Conference of Intelligent Robotic and Control Engineering (IRCE)*, 2018, pp. 1–5, doi: 10.1109/IRCE.2018.8492936.
- [7] C. C. Lindsey, “Form, function and locomotory habits in fish,” *Locomotion*, vol. 7, pp. 1–100, 1978, doi: 10.1016/s1546-5098(08)60163-6.
- [8] R. W. Blake, “Fish functional design and swimming performance,” *J. Fish Biol.*, vol. 65, no. 5, pp. 1193–1222, 2004.
- [9] J. J. Videler and F. Hess, “Fast continuous swimming of two pelagic predators, saithe (*Pollachius virens*) and mackerel (*Scomber scombrus*): a kinematic analysis,” *J. Exp. Biol.*, vol. 109, no. 1, pp. 209–228, 1984.
- [10] C. Zhou and K. H. Low, “Locomotion planning of biomimetic robotic fish with multi-joint actuation,” in *2009 IEEE/RSJ International Conference on Intelligent Robots and Systems*, 2009, pp. 2132–2137.
- [11] R. W. Blake, “Median and paired fin propulsion,” *Fish Biomech.*, vol. 1983, pp. 214–247, 1983.
- [12] L. Wang, S. Wang, Z. Cao, M. Tan, C. Zhou, H. Sang, and Z. Shen, “Motion control of a robot fish based on CPG,” in *2005 IEEE International Conference on Industrial Technology*, 2005, pp. 1263–1268.
- [13] J. Yu, M. Tan, J. Chen, and J. Zhang, “A survey on CPG-inspired control models and system implementation,” *IEEE Trans. Neural Networks Learn. Syst.*, vol. 25, no. 3, pp. 441–456, Mar. 2014, doi: 10.1109/TNNLS.2013.2280596.
- [14] A. R. Chowdhury, W. Xue, M. R. Behera, and S. K. Panda, “Hydrodynamics study of a BCF mode bioinspired robotic-fish underwater vehicle using Lighthill’s slender body model,” *J. Mar. Sci. Technol.*, vol. 21, no. 1, pp. 102–114, 2016.

- [15] B. G. Tong, "Propulsive mechanism of fish's undulatory motion," *Mech. Eng.*, vol. 22, no. 1, pp. 69–74, 2000.
- [16] D. R. Yoerger, J. G. Cooke, and J.-J. Slotine, "The influence of thruster dynamics on underwater vehicle behavior and their incorporation into control system design," *IEEE J. Ocean. Eng.*, vol. 15, no. 3, pp. 167–178, 1990.
- [17] H. Huang, C. Sheng, J. Wu, G. Wu, C. Zhou, and H. Wang, "Hydrodynamic analysis and motion simulation of fin and propeller driven manta ray robot," *Appl. Ocean Res.*, vol. 108, p. 102528, Mar. 2021, doi: 10.1016/j.apor.2021.102528.
- [18] G. Chen, X. Yang, X. Zhang, and H. Hu, "Water hydraulic soft actuators for underwater autonomous robotic systems," *Appl. Ocean Res.*, vol. 109, p. 102551, Apr. 2021, doi: 10.1016/j.apor.2021.102551.
- [19] T. Matsuda, R. Takizawa, T. Sakamaki, and T. Maki, "Landing method of autonomous underwater vehicles for seafloor surveying," *Appl. Ocean Res.*, vol. 101, Aug. 2020, doi: 10.1016/j.apor.2020.102221.
- [20] J. Glaze, R. Salazar, R. Vasconcellos, and A. Abdelkefi, "Comparative design, hydrodynamic analysis, and physical performance of fish-like robots," *Appl. Ocean Res.*, vol. 106, p. 102443, 2021, doi: <https://doi.org/10.1016/j.apor.2020.102443>.
- [21] G. Chen, X. Yang, X. Zhang, and H. Hu, "Water hydraulic soft actuators for underwater autonomous robotic systems," *Appl. Ocean Res.*, vol. 109, p. 102551, 2021, doi: 10.1016/j.apor.2021.102551.
- [22] H. Huang, C. Sheng, J. Wu, G. Wu, C. Zhou, and H. Wang, "Hydrodynamic analysis and motion simulation of fin and propeller driven manta ray robot," *Appl. Ocean Res.*, vol. 108, p. 102528, 2021, doi: 10.1016/j.apor.2021.102528.
- [23] J. Glaze, R. Salazar, R. Vasconcellos, and A. Abdelkefi, "Comparative design, hydrodynamic analysis, and physical performance of fish-like robots," *Appl. Ocean Res.*, vol. 106, p. 102443, Jan. 2021, doi: 10.1016/j.apor.2020.102443.
- [24] L. Zheng, S. Bi, Y. Cai, and C. Niu, "Design and optimization of a robotic fish mimicking cow-nosed ray," in *2010 IEEE International Conference on Robotics and Biomimetics*, 2010, pp. 1075–1080.
- [25] J. Gao, S. Bi, Y. Xu, and C. Liu, "Development and design of a robotic manta ray featuring flexible pectoral fins," in *2007 IEEE International Conference on Robotics and Biomimetics (ROBIO)*, 2007, pp. 519–523.
- [26] C. Niu, L. Zhang, S. Bi, and Y. Cai, "Development and depth control of a robotic fish mimicking cownose ray," in *2012 IEEE International Conference on Robotics and Biomimetics (ROBIO)*, 2012, pp. 814–818.
- [27] Y. Cai, S. Bi, and L. Zheng, "Design and experiments of a robotic fish imitating cow-nosed ray," *J. Bionic Eng.*, vol. 7, no. 2, pp. 120–126, 2010.
- [28] R. J. Clapham and H. Hu, "iSplash-I: High performance swimming motion of a carangiform robotic fish with full-body coordination," in *2014 IEEE International Conference on Robotics and Automation (ICRA)*, 2014, pp. 322–

327.

- [29] J. Yu, S. Chen, Z. Wu, and W. Wang, "On a miniature free-swimming robotic fish with multiple sensors," *Int. J. Adv. Robot. Syst.*, vol. 13, no. 2, p. 62, 2016.
- [30] G. Xie, L. Wang, and Y. Hu, "Multiple autonomous robotic fish collaboration," in *Robot Fish*, Springer, 2015, pp. 315–357.
- [31] S. Zhang, Y. Qian, P. Liao, F. Qin, and J. Yang, "Design and control of an agile robotic fish with integrative biomimetic mechanisms," *IEEE/ASME Trans. Mechatronics*, vol. 21, no. 4, pp. 1846–1857, 2016.
- [32] B. E. Flammang, J. L. Tangorra, A. P. Mignano, and G. V. Lauder, "Building a fish: the biology and engineering behind a bioinspired autonomous underwater vehicle," *Mar. Technol. Soc. J.*, vol. 51, no. 5, pp. 15–22, 2017.
- [33] R. Salazar, V. Fuentes, and A. Abdelkefi, "Classification of biological and bioinspired aquatic systems: A review," *Ocean Eng.*, vol. 148, pp. 75–114, 2018.
- [34] Y. Zhong, J. Song, H. Yu, and R. Du, "A Study on Kinematic Pattern of Fish Undulatory Locomotion Using a Robot Fish," *J. Mech. Robot.*, vol. 10, no. 4, p. 10, 2018.
- [35] J. Yu, S. Wang, and M. Tan, "Design of a free-swimming biomimetic robot fish," in *Proceedings 2003 IEEE/ASME International Conference on Advanced Intelligent Mechatronics (AIM 2003)*, 2003, vol. 1, pp. 95–100.
- [36] C. Beardsley, L. Bergeron, A. McLean, K. Nguyen, M. Vu, C. Watson, A. Nayfeh, H. Shehata, C. Woolsey, and M. Hajj, "A Modular Biocomotion Emulator for Hydrodynamic Testing in a Towing Tank," in *OCEANS 2018 MTS/IEEE Charleston*, 2018, pp. 1–8.
- [37] Z. Chen and X. Tan, "A Control-Oriented and Physics-Based Model for Ionic Polymer--Metal Composite Actuators," *IEEE/ASME Trans. Mechatronics*, vol. 13, no. 5, pp. 519–529, 2008.
- [38] Z. Chen, S. Shatara, and X. Tan, "Modeling of biomimetic robotic fish propelled by an ionic polymermetal composite caudal fin," *IEEE/ASME Trans. Mechatronics*, vol. 15, no. 3, pp. 448–459, 2010, doi: 10.1109/TMECH.2009.2027812.
- [39] L. Cen and A. Erturk, "Bio-inspired aquatic robotics by untethered piezohydroelastic actuation," *Bioinspir. Biomim.*, vol. 8, no. 1, p. 16006, 2013.
- [40] J. Wang, "Robotic fish: Development, modeling, and application to mobile sensing," Michigan State University. Electrical Engineering, Michigan, 2014.
- [41] R. 1942- Field, *Reef fishes : UAE and Gulf of Oman*. Dubai, United Arab Emirates: Motivate Publishing, 2005.
- [42] A. Agrawal, B. Prasad, V. Viswanathan, R. Kumar, and S. K. Panda, "Estimation and optimization of robotic fish design parameters for thrust velocity maximization," in *IECON 2013-39th Annual Conference of the IEEE Industrial Electronics Society*, 2013, pp. 4114–4119.

- [43] R. Salazar, A. Campos, V. Fuentes, and A. Abdelkefi, “A review on the modeling, materials, and actuators of aquatic unmanned vehicles,” *Ocean Eng.*, vol. 172, pp. 257–285, 2019, doi: <https://doi.org/10.1016/j.oceaneng.2018.11.047>.
- [44] “ITIS Standard Report Page: Apodichthys flavidus.” https://www.itis.gov/servlet/SingleRpt/SingleRpt?search_topic=TSN&search_value=171634#null (accessed Mar. 24, 2021).
- [45] A. Azuma, *The biokinetics of flying and swimming*, 2nd ed. Kawasaki, Kanagawa: American Institute of Aeronautics and Astronautics, 2006.
- [46] K. Matsuura, “OSTRACIIDAE Boxfishes (trunkfishes, cowfishes),” *living Mar. Resour. West. Cent. Atl.*, vol. 2, pp. 601–1374, 2002.
- [47] F. Santini, L. Sorenson, T. Marcroft, A. Dornburg, and M. E. Alfaro, “A multilocus molecular phylogeny of boxfishes (Aracnidae, Ostraciidae; Tetraodontiformes),” *Mol. Phylogenet. Evol.*, vol. 66, no. 1, pp. 153–160, 2013, doi: <https://doi.org/10.1016/j.ympev.2012.09.022>.
- [48] R. W. Blake, “On ostraciiform locomotion,” *J. Mar. Biol. Assoc. United Kingdom*, vol. 57, no. 4, pp. 1047–1055, 1977.
- [49] J. Yu and L. Wang, “Parameter optimization of simplified propulsive model for biomimetic robot fish,” in *Proceedings of the 2005 IEEE International Conference on Robotics and Automation*, 2005, pp. 3306–3311.
- [50] B. Siciliano, L. Sciavicco, L. Villani, and G. Oriolo, *Robotics: modelling, planning and control*. London: Springer Science & Business Media, 2010.
- [51] P. J. McKerrow and P. McKerrow, *Introduction to robotics*, vol. 3. Addison-Wesley Sydney, 1991.
- [52] “XM430-W350-T/R,” *Robotis*. <https://emanual.robotis.com/docs/en/dxl/x/xm430-w350/#position-pid-gain80-82-84> (accessed May 01, 2021).
- [53] M. J. Lighthill, “Aquatic animal propulsion of high hydromechanical efficiency,” *J. Fluid Mech.*, vol. 44, no. 2, pp. 265–301, 1970.
- [54] Z. Chen, P. Hou, and Z. Ye, “Robotic Fish Propelled by a Servo Motor and Ionic Polymer-Metal Composite Hybrid Tail,” *J. Dyn. Syst. Meas. Control. Trans. ASME*, vol. 141, no. 7, pp. 1–11, 2019, doi: 10.1115/1.4043101.
- [55] “ProJet 7000 HD - 3D Printer | 3D Systems.” <https://www.3dsystems.com/3d-printers/projet-7000-hd> (accessed Apr. 02, 2021).
- [56] D. Korkmaz, Z. H. Akpolat, S. Soygüder, and H. Alli, “Dynamic simulation model of a biomimetic robotic fish with multi-joint propulsion mechanism,” *Trans. Inst. Meas. Control*, vol. 37, no. 5, pp. 684–695, 2015.
- [57] Z. Chen, S. Shatara, and X. Tan, “Modeling of biomimetic robotic fish propelled by an ionic polymer--metal composite caudal fin,” *IEEE/ASME Trans. mechatronics*, vol. 15, no. 3, pp. 448–459, 2009.
- [58] B. W. Coad, “Family Pholidae – Gunnels, Sigouines,” B. W. Coad and J. D.

Reist, Eds. University of Toronto Press, 2019, pp. 528–529.

- [59] J. E. Randall and A. Cea, “JACKS (CARANGIDAE),” in *Shore Fishes of Easter Island*, University of Hawai’i Press, 2011, pp. 69–75.
- [60] X. Tan, D. Kim, N. Usher, D. Laboy, J. Jackson, A. Kapetanovic, J. Rapai, B. Sabadus, and X. Zhou, “An autonomous robotic fish for mobile sensing,” in *2006 IEEE/RSJ International Conference on Intelligent Robots and Systems*, 2006, pp. 5424–5429.
- [61] B. Kim, D.-H. Kim, J. Jung, and J.-O. Park, “A biomimetic undulatory tadpole robot using ionic polymer–metal composite actuators,” *Smart Mater. Struct.*, vol. 14, no. 6, p. 1579, 2005.
- [62] K. Takagi, M. Yamamura, Z.-W. Luo, M. Onishi, S. Hirano, K. Asaka, and Y. Hayakawa, “Development of a rajiform swimming robot using ionic polymer artificial muscles,” in *2006 IEEE/RSJ International Conference on Intelligent Robots and Systems*, 2006, pp. 1861–1866.
- [63] Z. Chen, T. I. Um, J. Zhu, and H. Bart-Smith, “Bio-inspired robotic cownose ray propelled by electroactive polymer pectoral fin,” in *ASME International Mechanical Engineering Congress and Exposition*, 2011, vol. 54884, pp. 817–824.
- [64] Z. Chen, T. I. Um, and H. Bart-Smith, “Ionic polymer-metal composite enabled robotic manta ray,” in *Electroactive Polymer Actuators and Devices (EAPAD) 2011*, 2011, vol. 7976, p. 797637.
- [65] Z. Wang, G. Hang, Y. Wang, J. Li, and W. Du, “Embedded SMA wire actuated biomimetic fin: a module for biomimetic underwater propulsion,” *Smart Mater. Struct.*, vol. 17, no. 2, p. 25039, 2008.
- [66] Z. Wang, Y. Wang, J. Li, and G. Hang, “A micro biomimetic manta ray robot fish actuated by SMA,” in *2009 IEEE International Conference on Robotics and Biomimetics (ROBIO)*, 2009, pp. 1809–1813.
- [67] W. Wang, J. Yu, R. Ding, and M. Tan, “Bio-inspired design and realization of a novel multimode amphibious robot,” in *2009 IEEE International Conference on Automation and Logistics*, 2009, pp. 140–145.
- [68] W. Wang and G. Xie, “CPG-based locomotion controller design for a boxfish-like robot,” *Int. J. Adv. Robot. Syst.*, vol. 11, no. 1, 2014, doi: 10.5772/58564.
- [69] R. Fan, J. Yu, L. Wang, G. Xie, Y. Fang, and Y. Hu, “Optimized design and implementation of biomimetic robotic dolphin,” in *2005 IEEE International Conference on Robotics and Biomimetics-ROBIO*, 2005, pp. 484–489.
- [70] K. Hirata and others, “Development of experimental fish robot,” in *Proceedings of The 6th International Symposium Marine Engineering (ISME 2000)*, 2000, pp. 23–27.
- [71] K. Hirata, T. Takimoto, and K. Tamura, “Study on turning performance of a fish robot,” in *First International Symposium on Aqua Bio-Mechanisms*, 2000, pp. 287–292.

- [72] J.-D. Liu and H. Hu, “Biologically inspired behaviour design for autonomous robotic fish,” *Int. J. Autom. Comput.*, vol. 3, no. 4, pp. 336–347, 2006.
- [73] H. Hu, “Biologically inspired design of autonomous robotic fish at Essex,” in *IEEE SMC UK-RI Chapter Conference, on Advances in Cybernetic Systems*, 2006, pp. 3–8.
- [74] K. H. Low, “Current and future trends of biologically inspired underwater vehicles,” in *2011 Defense Science Research Conference and Expo (DSR)*, 2011, pp. 1–8.
- [75] K. H. Low and C. W. Chong, “Parametric study of the swimming performance of a fish robot propelled by a flexible caudal fin,” *Bioinspiration & Biomimetics*, vol. 5, no. 4, p. 46002, 2010.
- [76] E. Papadopoulos, E. Apostolopoulos, and P. Tsigkourakos, “Design, control, and experimental performance of a teleoperated robotic fish,” in *2009 17th Mediterranean Conference on Control and Automation*, 2009, pp. 766–771.
- [77] D. Shin, S. Y. Na, J. Y. Kim, and S.-J. Baek, “Fish robots for water pollution monitoring using ubiquitous sensor networks with sonar localization,” in *2007 International Conference on Convergence Information Technology (ICCIT 2007)*, 2007, pp. 1298–1303.
- [78] D. Shin, S. Y. Na, J. Y. Kim, and S.-J. Baek, “Fuzzy neural networks for obstacle pattern recognition and collision avoidance of fish robots,” *Soft Comput.*, vol. 12, no. 7, pp. 715–720, 2008.

Vita

Mohamad Omari was born in 1996, in Beirut, Lebanon. He received his primary education in Beirut, Lebanon and his secondary education in Dubai, UAE. He received his B.Sc. degree in Mechanical Engineering from the American University of Sharjah in 2018.

In January 2019, he joined the Mechatronics Engineering master's program in the American University of Sharjah as a graduate teaching assistant, and later received the position of graduate research assistant under Dr. Mehdi Ghommem. His research interests are in control, cybernetics, mechatronics, and biomimicry.